IOP Publishing Journal of Geophysics and Engineering
J. Geophys. Eng. **13** (2016) 559–596 doi:10.1088/1742-2132/13/4/559

A new empirical method based on log-transformation regressions for the estimation of static formation temperatures of geothermal, petroleum and permafrost boreholes

O M Espinoza-Ojeda[1] **and E Santoyo**[2,3]

[1] CONACYT—Instituto de Investigaciones en Ciencias de la Tierra, Universidad Michoacana de San Nicolás de Hidalgo, Morelia, Michoacán 58060, México
[2] Instituto de Energías Renovables, Universidad Nacional Autónoma de México, Priv. Xochicalco s/n, Col. Centro, Temixco, Morelos 62580, México (Permanent address)
[3] Centro de Investigación en Ingeniería y Ciencias Aplicadas, Universidad Autónoma del Estado de Morelos, Av. Universidad 1001, Chamilpa, Cuernavaca 62100, Morelos, México (Temporary address)

E-mail: omespinozaoj@conacyt.mx and esg@ier.unam.mx (E Santoyo)

Received 15 November 2015, revised 25 April 2016
Accepted for publication 24 May 2016
Published 15 July 2016

Abstract

A new practical method based on logarithmic transformation regressions was developed for the determination of static formation temperatures (SFTs) in geothermal, petroleum and permafrost bottomhole temperature (BHT) data sets. The new method involves the application of multiple linear and polynomial (from quadratic to eight-order) regression models to BHT and log-transformation (T*ln*) shut-in times. Selection of the best regression models was carried out by using four statistical criteria: (i) the coefficient of determination as a fitting quality parameter; (ii) the sum of the normalized squared residuals; (iii) the absolute extrapolation, as a dimensionless statistical parameter that enables the accuracy of each regression model to be evaluated through the extrapolation of the last temperature measured of the data set; and (iv) the deviation percentage between the measured and predicted BHT data. The best regression model was used for reproducing the thermal recovery process of the boreholes, and for the determination of the SFT. The original thermal recovery data (BHT and shut-in time) were used to demonstrate the new method's prediction efficiency. The prediction capability of the new method was additionally evaluated by using synthetic data sets where the true formation temperature (TFT) was known with accuracy. With these purposes, a comprehensive statistical analysis was carried out through the application of the well-known *F*-test and Student's *t*-test and the error percentage or statistical differences computed between the SFT estimates and the reported TFT data.

After applying the new log-transformation regression method to a wide variety of geothermal, petroleum, and permafrost boreholes, it was found that the polynomial models were generally the best regression models that describe their thermal recovery processes. These fitting results suggested the use of this new method for the reliable estimation of SFT. Finally, the practical use of the new method was highlighted because it only requires the use of BHT and shut-in time measurements as the main input data, which represents an enormous advantage over most of the analytical methods reported in the literature that require a large number of measurements (e.g. circulation time, the thermophysical and transport properties of the formation or drilling fluid, among others).

Keywords: static formation temperature, bottomhole temperatures, shut-in time, log-transformation, linear and polynomial regression models, geothermal energy

(Some figures may appear in colour only in the online journal)

1. Introduction

Previous research works in the worldwide literature have demonstrated that the reliable estimation of stabilized formation temperatures (SFTs) in geothermal and petroleum systems has relevance in the evaluation of geoenergy reserves (Santoyo *et al* 2000, Olea-González *et al* 2007, Kutasov and Eppelbaum 2011). Moreover, in climatic change studies, the determination of SFT in permafrost boreholes also exhibits scientific relevance to elucidating temperature changes on the Earth, specifically those related to surface temperature increases (Lachenbruch and Marshall 1986, Harris and Chapman 1997, Huang *et al* 2000).

The estimation of SFT from transient bottomhole temperature (BHT) measurements provides the opportunity to determine the virgin temperatures of the surrounding formation-rock during the thermal recovery processes of the borehole. For this reason, it is conceived of as a valuable tool in terms of planning, exploration, evaluation and developing geothermal, petroleum and permafrost projects (Verma *et al* 2006a, Bodri and Cermak 2007, Kutasov and Eppelbaum 2010).

In this context, numerical simulators and simplified analytical methods (based on heat transfer models) were initially developed for the thermal study of petroleum boreholes under drilling and completion conditions, and later extended to both the geothermal industry and to the study of the thermal history of permafrost zones (e.g. Harris and Chapman 1997, Davis *et al* 2011). Numerous simulators have been specifically developed for the determination of the complete thermal history of a drilled borehole and the surrounding rock-formation under a wide variety of heat transfer models and assumptions (Pioneer works: e.g. Raymond 1969, Keller *et al* 1973, Beirute 1991 and recent works: e.g. Olea-González *et al* 2007, 2008, Olea-González and García-Gutiérrez 2008, Espinosa-Paredes *et al* 2009, Porkhial *et al* 2015, Yang *et al* 2015).

On the other hand, a large number of analytical methods have been reported in the same literature for the estimation of the SFT in geothermal, petroleum, and permafrost boreholes (e.g. the pioneer works by Dowdle and Cobb 1975, Leblanc *et al* 1981; and recent contributions such as those reported by Bassam *et al* 2010, Wong-Loya *et al* 2012, 2015; among others). In the context of practical analytical tools, several works have criticized the validity of some analytical methods for calculating SFT in these geosystems (Luheshi 1983, Drury 1984, Shen and Beck 1986, Deming 1989, Andaverde *et al* 2005, Espinoza-Ojeda *et al* 2011). These studies have demonstrated that some simplified analytical methods were derived under unrealistic heat transfer assumptions, and with a wrong use of linear regression models in the simplified solutions to estimate the SFT. Significant errors have been actually reported when these analytical methods were used to estimate the SFT using synthetic BHT data sets, where the true formation temperature (TFT) is known with accuracy (e.g. Drury 1984, Andaverde *et al* 2005, Verma *et al* 2006a). In addition, large discrepancies have also been reported among the SFT estimates predicted by several analytical methods using the same BHT data sets (e.g. Santoyo *et al* 2000, Espinoza-Ojeda *et al* 2011, Wong-Loya *et al* 2012).

These conceptual (physical and statistical) problems explain why some analytical methods systematically show a tendency either to underestimate (e.g. the Horner-plot method: Dowdle and Cobb 1975) or overestimate (e.g. the spherical–radial method: Ascencio *et al* 1994) the SFT. However, in spite of these problems, some of these analytical methods are still being used in the geothermal and petroleum industry, probably for their simplicity in the calculation of SFT (e.g. Espinosa-Paredes and García-Gutiérrez 2003, Kutasov and Eppelbaum 2005, Goutorbe *et al* 2007, Pasquale *et al* 2008, Kutasov and Eppelbaum 2010, Eppelbaum and Kutasov 2011, Vaz de Medeiros Rangel 2014, Sulastri and Andriany 2015).

To overcome the conceptual problems detected with the use of previous analytical methods, and the necessity of additional information (e.g. the thermophysical and transport properties of drilling materials: mud, cement, rock-formation, etc), which is rarely available in drilling logging, a new empirical method to estimate SFT by using only transient BHT data sets logged from geothermal, petroleum, and permafrost boreholes has been developed. The new method performs analysis of transient BHT measurements (logged during borehole shut-in conditions) by applying an innovative mathematical methodology based on logarithmic transformation regressions. The SFT is estimated after reproducing the typical transient asymptotic behavior of BHT measurements (also called thermal recovery or the shut-in process) by assuming that the formation has reached a thermal equilibrium state at infinite time. The aim of this paper is to describe the mathematical basis of the new empirical method, the numerical algorithm used, and some application examples for demonstrating the effective and reliable prediction task of the SFT.

2. The new empirical method

The main goal of this work is to reproduce the thermal recovery behavior of geothermal, petroleum and permafrost boreholes from the analysis of transient BHT data logged during their drilling and completion operations. For these purposes, borehole thermal recovery (also named shut-in) occurs after either cooling or heating the surrounding rock-formation by the drilling fluid circulation in the case of geothermal–petroleum

or permafrost systems, respectively. After the thermal disturbance caused by the drilling process, rock-formation temperatures begin to increase in geothermal or petroleum systems, whereas in permafrost systems, a reverse tendency is observed in the borehole temperature profiles. The typical behavior pattern obtained under thermal recovery conditions generally exhibits an asymptotic curve, which can be observed by plotting the BHT versus shut-in time data (e.g. figures 2–14). The same process can also be observed in the estimation of the initial reservoir pressure of petroleum and geothermal boreholes, which commonly exhibit a similar recovery process at infinity time (e.g. Horner 1951, Fertl and Timko 1972, Grant *et al* 1983, Cao and Lerche 1990, Barelli *et al* 1994, Aragón *et al* 1999, Stevens 2000).

The thermal recovery observed during borehole drilling operations has been extensively studied by heat transfer models (conductive and convective), which have been applied to derive simplified analytical methods that are commonly used to reproduce the asymptotic tendency between BHT and shut-in time data, and hence, to determine the SFT in geothermal and petroleum boreholes.

Radial, cylindrical and spherical conductive models have been used to derive simplified analytical methods (e.g. Manetti 1973, Ascencio *et al* 1994), whereas radial and cylindrical convective models have also been employed to obtain other analytical tools (e.g. Hasan and Kabir 1994).

Other heat transfer models have been additionally oriented to studying the asymptotic behavior of BHT and shut-in time data (e.g. Middleton 1979, 1982, Barelli and Palama 1981, Leblanc *et al* 1981, Lee 1982, Luheshi 1983, Jones *et al* 1984, Ribeiro and Hamza 1986, Shen and Beck 1986, Cao *et al* 1988a, 1988b, Beirute 1991, Waples and Ramly 1995, 2001, Waples and Pederson 2004, Waples *et al* 2004a, 2004b).

For analyzing thermal recovery in a reliable way, the number of BHT data available for performing these calculations has been one of the major concerns of these tasks. In relation to this, and as a result of the high cost of well logging operations, most of the BHT measurements logged in petroleum and geothermal boreholes are usually not numerous, and commonly available in the interval of 3–10 measurements (e.g. Pasquale *et al* 2008). Temperature logging is usually carried out under short shut-in times (<30 h). Longer transient BHT data are sometimes collected in exploration exceptional cases (<200 h). In the case of permafrost systems (where most boreholes are drilled for research purposes), transient BHT measurements are commonly logged at long shut-in times (from a hundred to a thousand days), but with the same problem of having a limited number of BHT measurements.

On the other hand, the asymptotic curve pattern associated with the thermal recovery process may be alternatively reproduced by means of mathematical functions such as logarithmical, exponential or polynomial models (e.g. Espinoza-Ojeda 2011, Wong-Loya *et al* 2012, 2015). The use of regression models based on a logarithmic transformation of variables (either x or y) for reproducing the asymptotic tendencies among them has been previously reported in the literature (e.g. Baskerville 1972, Howarth and Earle 1979). More recently, Verma and Quiroz-Ruiz (2008), Verma (2009, 2015), and Verma and Agrawal (2011) published some works which proposed the use of logarithmic transformation in polynomial regression to obtain more precise critical values to be used in discordance and significance (F- and Student's t-) statistical tests. This methodology was proposed because the critical values also exhibit asymptotic patterns that can be accurately reproduced by using a logarithmic transformation model as the most suitable regression tool both to interpolate and to extrapolate such data.

All these previous applications motivated the use of different regression models based on a logarithmic transformation of the independent variable (i.e. shut-in time) for a better fitting process of transient BHT measurements, and from this, to reproduce more accurately the typical thermal recovery behavior observed in drilled boreholes (geothermal, petroleum or permafrost). The fitting capability of these mathematical functions enabled the new empirical method to be developed as an innovated and improved analytical method. With this new regression tool the asymptotic behavior of BHT measurements with shut-in times was successfully reproduced, and finally used to determine the SFT with precision and accuracy.

The new empirical method proposes the application of a logarithmic transformation (Tln) in a regression model (GRM) that is either linear or polynomial, which can be represented by the following generalized equation:

$$y(x) = \sum_{i-0}^{m} a_i x^i \tag{1}$$

where y represents the dependent variable (BHT), x the independent variable (Δt or shut-in time), and a_i the coefficients of the regression model. As an initial step, three different logarithmic transformations (Tln) should be applied to the independent variables of the GRM to obtain three new improved independent variables (i.e. single (Tln1), double (Tln2), and triple (Tln3) functions which determine the new values of the independent variable: ($ln\ \Delta t$); $ln(ln\ \Delta t)$; and $ln(ln(ln\ \Delta t))$, respectively). The main hypothesis of the new empirical method assumes that by applying linear or polynomial regression models to the BHT and the improved shut-in time data, the SFT will be estimated at infinite time conditions. Based upon the number of BHT data measurements, initially, it proposed the application of the GRM maximum order (different regression models) as the applicability criterion of the new empirical method. Based upon the fit results and the calculated residuals, the best regression model was selected to determine the SFT. These SFT estimates were compared with those SFT values predicted by some of the analytical methods commonly used in the geothermal and petroleum industry.

3. Work methodology

To derive the new empirical analytical method, a statistical–numerical methodology was proposed. The work methodology is schematically represented through the schematic flow diagram of figure 1. Basically the methodology consists of the following numerical and statistical tasks:

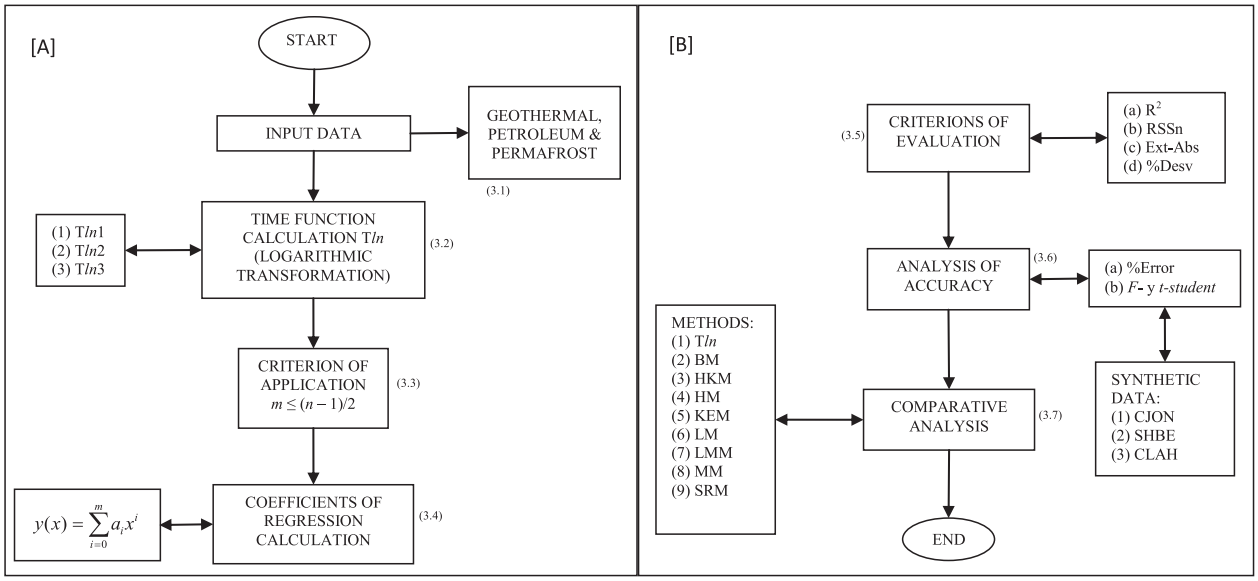

Figure 1. Flow diagram of the work methodology (numeric–statistical) used for the application of the new log-transformation method. (A) Steps to apply the log-transformation (T*ln*) method; (B) steps to evaluate statistically the T*ln* numerical results.

(1) To create a worldwide database from the BHT and shut-in time measurement logs of drilled boreholes. The database specifically consists of transient BHT data sets logged from 16 geothermal, 8 petroleum, and 3 permafrost boreholes, and 3 synthetic data sets where the TFT is known with accuracy.

(2) To apply the logarithmic transformation (T*ln*) functions (T*ln*1, T*ln*2, and T*ln*3) to the shut-in time data associated with each BHT data set, which will define the new improved value of the independent variable (equation (1)).

(3) To apply the applicability criterion to the maximum order of the GRM, which is defined as $m \leqslant (n-1)/2$, where m and n are the maximum order of the regression model to be used, and the total number of BHT data, respectively. This first applicability criterion also allows the maximum order of the polynomial model (in the GRM) based on the total number of data sets to be evaluated. The nomenclature to determine the polynomial models to be used in the GRM (equation (1)) was as follows: linear (*L*); quadratic (*Q*); cubic (*C*); fourth (FO); fifth (FI); sixth (SI); seventh (SE); and eighth (EI).

(4) To calculate the GRM coefficients of equation (1) by using the regression numerical routines included in the commercial software STATISTICA (StatSoft 2003).

(5) To select the best GRM model that allows the reproduction of the BHT data with reliability, and hence, the estimation of the SFT at infinite recovery time ($\Delta t \rightarrow \infty$) by using the following statistical criteria of evaluation:

- *Coefficient of determination* (R^2). From a statistical point of view, the parameter R^2 was used to evaluate the quality of the regression in terms of the variation between two variables (x and y) to be correlated in any regression model. This parameter is calculated for each regression model using the complete BHT data set, and a numerical value that approaches the unit will be expected when the regression is statistically acceptable ($R^2 \approx 1$: Bevington and Robinson 2003).
- *Sum of the normalized squared residuals* (RSSn). The different regression models applied to the relationship BHT–improved shut-in time (modified by the logarithmically transformed function (T*ln*)) were also evaluated through the estimation of the well-known statistical parameter RSSn. The best fit model will be given by the smaller RSSn numerical values. The RSSn was estimated by means of the equation:

$$\mathrm{RSSn} = \frac{\sum_{i=1}^{n}(\mathrm{BHT}_i - T_i)^2}{n} \tag{2}$$

where BHT_i and T_i are the measured and calculated (predicted by the new empirical method) transient temperatures, respectively.

- *Absolute extrapolation* (Ext-Abs). A dimensionless statistical parameter that enables the accuracy of each regression model to be evaluated through the extrapolation of the last temperature measured (BHT_n) of the data set. The results of each GRM (with T*ln*) were compared to determine the best BHT_n predictor through the calculation of a dimensionless absolute difference between the measured BHT_n and the predicted T_n by the GRM (with T*ln*). In this case, the evaluation criterion establishes the small numerical value of the parameter Ext-Abs belongs to the best predictor of BHT_n. The parameter Ext-Abs was calculated as:

$$\text{Ext-Abs} = \left| \frac{\mathrm{BHT}_n - T_n}{\mathrm{BHT}_n} \right| \tag{3}$$

- *Deviation percentage* (%Dev). The dimensionless parameter %Dev is a combination of conditions used to calculate the SFT estimates and their associated uncertainty. All the different regression models (GRM with T*ln*) obtained in each BHT data set were

simulated numerically at long times ($\Delta t \rightarrow \infty$). In each analyzed data set, the BHT_n was used as reference data to determine the SFT. The dimensionless parameter %Dev was determined by means of the following equation:

$$\%\text{Dev} = \left| \frac{T_{i+1} - T_i}{T_{i+1}} \right| \times 100 \tag{4}$$

For the analysis of geothermal and petroleum cases, and according to the temperature magnitude, $\%\text{Dev} \leqslant 0.01$ was used as a strict convergence criterion for estimating the SFT through the numerical simulation of each GRM ($T\ln$) at infinite time. This means that in the case of using the value 0.01, if the numerical simulation does not accomplish the complementary conditions, the next value (0.001) will be used, and so on. The complementary condition to be accomplished in geothermal and petroleum application cases is that the SFT calculated at infinite time by the new method must be greater than the last BHT measured data ($\text{SFT}(T\ln) > \text{BHT}_n$). For the analysis of permafrost boreholes, a value of $\%\text{Dev} \leqslant 0.001$ was defined according to the BHT and long Δt data, which acts as a complementary condition for the estimation of the SFT using an inverse condition: $\text{SFT}(T\ln) < \text{BHT}_n$. The general complementary condition to the systems under analysis was the simulation time (Δt_{n+i}) and in order to obtain the SFT by these means, the new method simulation time ($T\ln(\Delta t_{n+i})$) must be greater than the BHT_n shut-in time (Δt_n) measurements ($T\ln(\Delta t_{n+i}) > \Delta t_n$).

For the determination of the SFT which corresponds to the BTH data sets under evaluation, the four statistical evaluation criteria were together applied both to decide the best GRM to fit the analyzed BHT and to reproduce the thermal recovery behavior of each data set. The results of the statistical evaluation parameters (R^2, RSSn, Ext-Abs and %Dev) were reported with the greatest possible number of digits to facilitate the final analysis of the selection. However, the SFT estimated by means of this numerical procedure was reported with the number of significant digits imposed by the uncertainty associated with the new method.

(6) For the accuracy analysis of the new empirical method, three synthetic data sets (CJON, SHBE and CLAH), were used because in these series the 'true' SFT (TFT) was known. TFT was therefore used as the reference parameter of accuracy evaluation. With this in mind, the next accuracy parameters were additionally calculated: (a) the error percentage (%Error) existing between the SFT calculated by the new method and the TFT reported for the synthetic data; and (b) the significant differences between the calculated SFT and the TFT by applying the statistical tests of *F*- and Student's *t*-.

(7) Two different types of comparative statistical analyses were finally carried out between the SFT values calculated by the new empirical method and those SFT estimates inferred from eight alternative analytical methods (already reported in the literature) using their approximated or simplified solutions with ordinary least-square (OLS) and quadratic regression (QR) models. These comparative analyses were performed by the following statistical procedures:

(7.1) A comparative analysis of the SFT estimates between the values inferred from other analytical methods and those predicted from the new empirical method. For geothermal and petroleum borehole cases, the SFT calculated by the new method was always higher than the last BHT_n, which avoids an underestimation of the SFT, whereas for permafrost applications, the SFT estimated must always be lower than the last BHT_n; and

(7.2) A comparative analysis between the SFT estimates predicted by the new empirical method and the mean values calculated from the SFT values inferred by the eight analytical methods. For the calculation of the mean SFT value and the associated standard deviation, a statistical normalization process was performed by using the computer software DODESYS, which uses discordant tests of univariate data to ensure Gaussian distributions of the SFT estimates (Verma *et al* 2008). The mean SFT estimated in each data set was finally compared with the predicted value by the new method using the *F*- and Student's *t*-statistical tests.

For the purposes of the comparative analyses (7.1 and 7.2), the following simplified analytical methods were used for the determination of SFT:

(i) the conductive radial heat source or Brennand method (BM: Brennand 1984);
(ii) the conductive–convective cylindrical heat source or Hasan–Kabir method (HKM: Hasan and Kabir 1994);
(iii) the constant linear heat source or Horner-plot method, (HM: Timko and Fertl 1972, Dowdle and Cobb 1975);
(iv) the generalized Horner or Kutasov–Eppelbaum method (KEM: Kutasov and Eppelbaum 2005);
(v) the conductive cylindrical heat source or Leblanc method (LM: Leblanc *et al* 1981);
(vi) the rectangular heat source or Leblanc–Middleton method (LMM: proposed by Middleton 1979 and improved by Leblanc *et al* 1982);
(vii) the conductive cylindrical heat source or Manetti method (MM: Manetti 1973); and
(viii) the spherical–radial heat flow method (SRM: Ascencio *et al* 1994).

Instead of providing details on the theory of each method in the present work, the reader is referred to the original literature source of each model or method for other physical, mathematical or assumption details.

4. Results and discussion

4.1. Creation of a world database

A world database containing sixteen BHT data sets logged during borehole drilling operations, and three synthetic (experimental)

Table 1. Data sets used for the calculation of SFT through log-transformation method and eight commonly used analytical methods.

Data sets	Data Number	Maximum order of the GRM ($m \leqslant (n-1)/2$)	Reference
Geothermal boreholes:			
CH-A_4 (948 m)	6	2nd	González-Partida *et al* (1997)
CH-A_9 (2198 m)	6	2nd	González-Partida *et al* (1997)
CH-A_{11} (2298 m)	6	2nd	González-Partida *et al* (1997)
$MXCO_1$	6	2nd	Verma *et al* (2008)
$MXCO_2$	7	3rd	Verma *et al* (2008)
ITAL	40	8th	Da-Xin (1986)
PHIL	14	6th	Brennand (1984)
JAPN (700 m)	10	4th	Hyodo and Takasugi (1995)
CB-1 (994 m)	4	Linear	Ascencio *et al* (2006)
CB-1 (1494 m)	3	Linear	Ascencio *et al* (2006)
CB-1 (1987 m)	3	Linear	Ascencio *et al* (2006)
CB-1 (2583 m)	4	Linear	Ascencio *et al* (2006)
R#9-1 (1518 m)	7	3rd	Crosby (1977)
SGIL	12	5th	Schoeppel and Gilarranz (1966)
GT-2 (1595 m)	77	8th	Albright (1975)
ROUX (1518 m)	3	Linear	Roux *et al* (1980)
KELLEY (1035 m)	3	Linear	Roux *et al* (1980)
Synthetic data:			
CJON	12	5th	Cooper and Jones (1959)
SHBE	8	3rd	Shen and Beck (1986)
CLAH	15	7th	Cao *et al* (1988a)
Petroleum boreholes:			
USAM (4900 m)	14	6th	Kutasov (1999)
COST (1420 m)	6	2nd	Cao *et al* (1988b)
COST (3710 m)	5	2nd	Cao *et al* (1988b)
COST (4475 m)	4	Linear	Cao *et al* (1988b)
MALOOB-456	9	4th	Espinosa-Paredes *et al* (2009)
MALOOB-309D	7	3rd	Espinosa-Paredes *et al* (2009)
PPH-ABA (3328 m)	4	Linear	Pasquale *et al* (2008)
BECU (2700 m)	5	2nd	Beardsmore and Cull (2001)
Permafrost boreholes:			
REINDEER	10	4th	Taylor *et al* (1982)
MOKKA	9	4th	Taylor *et al* (1982)
P-RIVER	9	4th	Clow and Lachenbruch (1998)

Note: The number of BHT measurements and the maximum order of the regression models for their application are also included.

data sets was created (see table 1). These data sets were compiled from borehole drilling reports on geothermal, petroleum and permafrost systems:

For the case of temperature measurements logged from geothermal boreholes, 11 boreholes drilled in different world geothermal fields were compiled. These geothermal boreholes are described in the following list together with the acronym we used, the location and the maximum shut-in time recorded:

(1) Chipilapa, El Salvador (CH-A, with shut-in times up to 190.5 h);

Table 2. Statistical evaluation parameters R^2, RSSn, and Ext-Abs and the SFT estimated for the regression models (GRM (T*ln*)) of the geothermal data set CH-A_9 (using as rigorous value %Dev $\leqslant 0.01$ for the numerical simulation).

Model	R^2	RSSn	Ext-Abs	SFT (°C)
L (T*ln*1)	0.995 663	0.981 68	0.001 733	156.462 92
Q (T*ln*1)	0.997 336	0.603 01	0.029 612	164.049 63
L (T*ln*2)	0.956 859	9.764 196	0.044 806	140.838 84
Q (T*ln*2)	0.998 68	0.298 777	0.012 476	156.518 24
L (T*ln*3)	0.877 831	27.650 918	0.077 915	138.960 73
Q (T*ln*3)	0.995 55	1.007 078	0.010 67	148.035 45

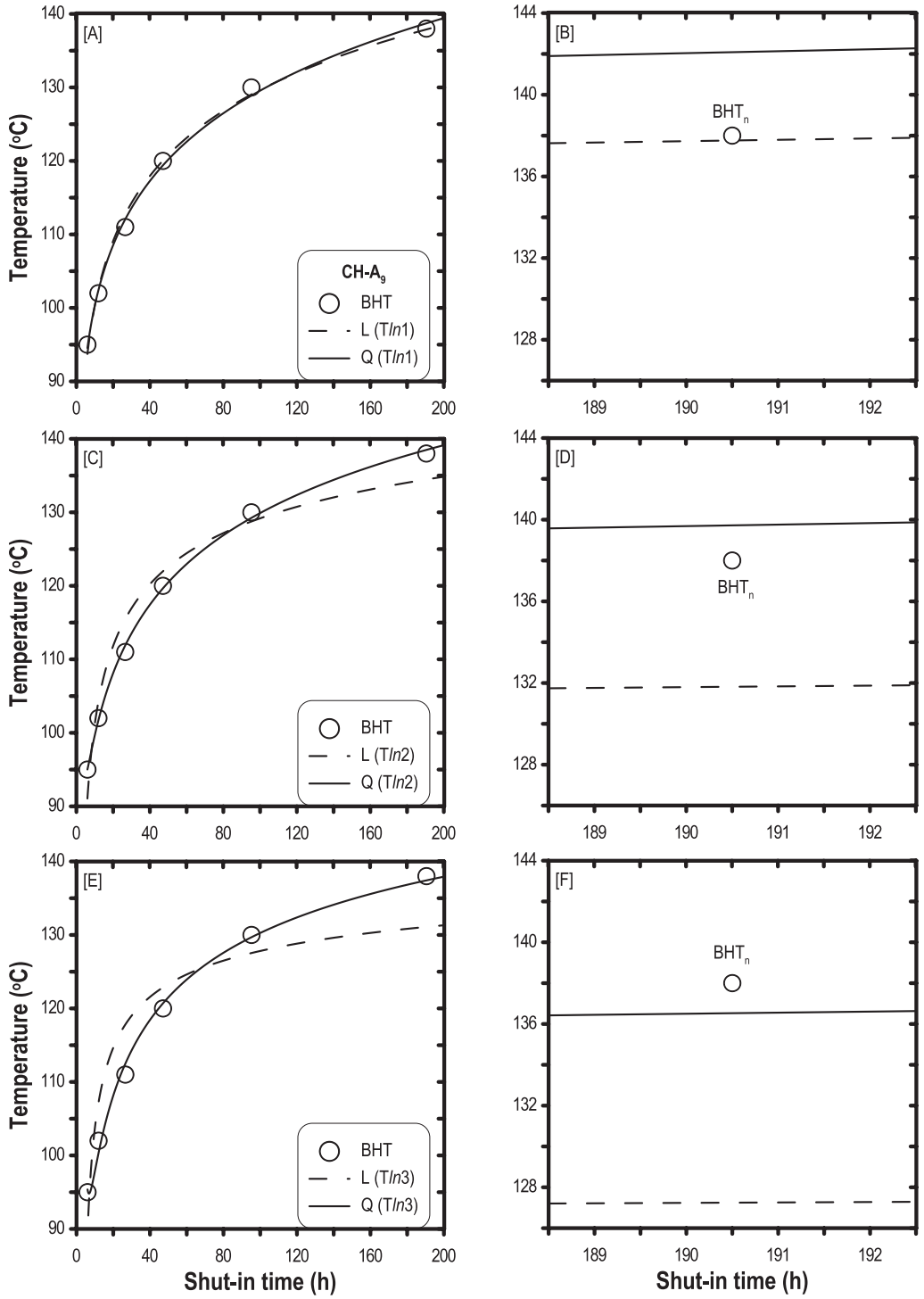

Figure 2. Integrated numerical simulation used for the regression models applied to geothermal data set CH-A9: (A) $L(T\ln 1)$ and $Q(T\ln 1)$; (C) $L(T\ln 2)$ and $Q(T\ln 2)$; and (E) $L(T\ln 3)$ and $Q(T\ln 3)$. BHT_n and numerical approximation plots obtained for the Ext-Abs parameter analysis: (B) $L(T\ln 1)$ and $Q(T\ln 1)$; (D) $L(T\ln 2)$ and $Q(T\ln 2)$; and (F) $L(T\ln 3)$ and $Q(T\ln 3)$.

(2) Los Humeros, México (MXCO, with shut-in times up to 36 h and 42 h);
(3) Larderello, Italy (ITAL, with shut-in times up to 27 h);
(4) Philippines (PHIL, with shut-in times up to 15.58 h);
(5) Kyushu, Japan (JAPN, with shut-in times up to 72.5 h);
(6) Ceboruco, México (CB-1, with shut-in times up to 24 h);
(7) Roosevelt, USA (R #9-1, with shut-in times up to 46 h);
(8) Oklahoma, USA (SGIL, with shut-in times up to 12 h);
(9) New Mexico, USA (GT-2, with shut-in times up to 44 h);
(10) Imperial Valley, USA (ROUX, with shut-in times up to 13.5 h); and
(11) Kelley Hot Spring, USA (KELLEY, with shut-in times up to 29.3 h).

For the accuracy evaluation of the new log-transformation method, three well-known synthetic data sets were

Table 3. A summary of the numerical results obtained for the application of the new method to the geothermal data sets CH-A_4, CH-A_{11}, $MXCO_1$, $MXCO_2$, ITAL, PHIL, JAPN and R #9-1 (using as rigorous value %Dev $\leqslant 0.01$ for the SFT numerical prediction).

Model	R^2	RSSn	Ext-Abs	SFT (°C)
CH-A_4 ($n = 6$, $BHT_n = 169$ °C)				
Q (T*ln*3)	0.996 722	2.956 543	0.001 296	194.916 32
L (T*ln*2)	0.964 099	32.376 074	0.053 473	181.4573
L (T*ln*3)	0.892 873	96.607 761	0.108 527	175.047 61
CH-A_{11} ($n = 6$, $BHT_n = 145$ °C)				
Q (T*ln*2)	0.996 878	0.785 206	0.027 293	172.059 23
Q (T*ln*3)	0.996 684	0.833 766	0.005 419	158.900 02
Q (T*ln*1)	0.988 733	2.833 226	0.058 883	191.930 27
$MXCO_1$ ($n = 6$, $BHT_n = 247.7$ °C)				
Q (T*ln*3)	0.996 613	1.460 254	0.009 664	320.090 27
L (T*ln*3)	0.920 687	34.194 589	0.044 714	262.985 46
L (T*ln*2)	0.967 773	13.894 016	0.029 139	290.549 15
$MXCO_2$ ($n = 7$, $BHT_n = 247.1$ °C)				
C (T*ln*1)	0.998 045	1.017 936	0.000 701	274.976 16
C (T*ln*3)	0.997 908	1.088 956	0.003 577	354.613 97
L (T*ln*3)	0.796 159	51.260 305	0.096 799	262.197 53
ITAL ($n = 39$, $BHT_n = 118.7$ °C)				
SI (T*ln*3)	0.999 832	0.008 434	0.002 586	119.832 27
SI (T*ln*2)	0.999 82	0.009 014	0.002 446	119.702 77
PHIL ($n = 14$, $BHT_n = 146$ °C)				
C (T*ln*2)	0.989 219	3.375 62	0.040 132	178.8161
L (T*ln*3)	0.910 849	24.476 029	0.079 313	158.406 08
L (T*ln*2)	0.892 521	33.652 404	0.071 256	183.4237
JAPN ($n = 10$, $BHT_n = 170.9$ °C)				
FO (T*ln*2)	0.999 962	0.019 106	0.014 319	176.437 47
FO (T*ln*1)	0.999 943	0.029 189	0.186 46	171.092 71
FO (T*ln*3)	0.999 889	0.056 454	0.048 056	201.353 17
R #9-1 ($n = 7$, $BHT_n = 170$ °C)				
C (T*ln*3)	0.997 299	0.242 136	0.017 264	196.104 66
C (T*ln*2)	0.997 245	0.247	0.018 191	381.457 47
Q (T*ln*3)	0.997 153	0.255 235	0.000 013	172.920 47

additionally used. These synthetic data sets are reported in table 1 (CJON, $n = 12$; SHBE, $n = 8$; and CLAH, $n = 15$; with shut-in times up to 1.5 h, 40 h, and 50 h, respectively), which were collected from experimental works performed by Cooper and Jones (1959), Shen and Beck (1986), and Cao *et al* (1988b), respectively. The corresponding TFT values reported for these data sets were CJON = 20.25 °C, SHBE = 80.0 °C, and CLAH = 120.0 °C.

For the case of temperature measurements logged from petroleum boreholes, the following sites were also compiled in the worldwide database:

(12) Mississippi, USA (USAM, with shut-in times up to 200 h);
(13) Norton Sound, US (COST, with shut-in times up to 75.5 h);
(14) Gulf of Mexico, Mexico (MALOOB, with longer shut-in times up to 5184 h);
(15) Po Plain, Italy (PPH-ABA, with shut-in times up to 36.5 h);
(16) Browse Basin, Australia (BECU, with shut-in times up to 18.3 h).

Table 4. A summary of the numerical results obtained for the application of the new method to the geothermal data sets CB-1, SGIL, ROUX and KELLEY (using as rigorous value %Dev $\leqslant 0.01$ for the SFT numerical prediction).

Model	R^2	RSSn	Ext-Abs	SFT (°C)
CB-1 (994 m) ($n = 4$, $BHT_n = 52.3$ °C)				
L (T*ln*1)	0.979 109	0.022 249	0.002 719	57.565 91
L (T*ln*2)	0.965 923	0.036 292	0.001 377	54.488 601
L (T*ln*3)	0.936 624	0.067 496	0.005 306	53.219 369
CB-1 (1494 m) ($n = 3$, $BHT_n = 65.8$ °C)				
L (T*ln*2)	0.998 433	0.012 299		78.473 125
L (T*ln*3)	0.992 25	0.060 828		72.811 573
CB-1 (1987 m) ($n = 3$, $BHT_n = 90$ °C)				
L (T*ln*2)	0.979 413	0.279 573		98.063 551
L (T*ln*3)	0.944 743	0.750 396		93.341 348
CB-1 (2583 m) ($n = 4$, $BHT_n = 102.7$ °C)				
L (T*ln*3)	0.905 541	3.555 599	0.048 389	108.479 79
SGIL ($n = 12$, $BHT_n = 96.13$ °C)				
FO (T*ln*3)	0.998 917	0.005 393	0.002 418	101.803 52
C (T*ln*3)	0.998 816	0.005 896	0.002 224	99.8027
Q (T*ln*3)	0.998 78	0.006 073	0.001 518	100.063 15
ROUX ($n = 3$, $BHT_n = 155.56$ °C)				
L (T*ln*3)	0.990 872	0.368 253		179.869 65
L (T*ln*2)	0.982 425	0.709 079		199.781 08
L (T*ln*1)	0.972 76	1.098 997		252.543 85
KELLEY ($n = 3$, $BHT_n = 94.44$ °C)				
L (T*ln*3)	0.989 185	0.202 301		112.233 54
L (T*ln*1)	0.997 895	0.039 367		145.889 75
L (T*ln*2)	0.994 087	0.110 598		121.598 46
GT-2 (1595 m) ($n = 77$, $BHT_n = 123.817$ °C)				
SE (T*ln*3)	0.999 72	0.122 01	0.000 121	123.832 32
FI (T*ln*3)	0.999 563	0.190 541	0.000 068	124.212 13
SI (T*ln*3)	0.999 587	0.179 983	0.000 135	137.162 91

Finally, for the case of permafrost borehole temperatures, thermal recovery measurements were compiled from three different exploration sites, which included thermal data logged at distinct depths:

(17) Reindeer D-27, Canada (REINDEER, 9 different depths with shut-in times up to 4577 d);
(18) Mokka A-02, Canada (MOKKA, 11 different depths with shut-in times up to 6884 d);
(19) Put River N-1, Alaska, US (P-RIVER, 14 different depths with shut-in times up to 1071 d).

Table 1 summarizes all the information sources from where the data sets were originally compiled for the three application areas: geothermal, petroleum and permafrost.

4.2. Logarithmic transformation

According to the GMR (equation (1)), the application of the logarithmic transformation (T*ln*: T*ln*1; T*ln*2; T*ln*3) to the independent variable (x: Δt shut-in time) was defined as follows: (i) a simple logarithmic transformation (T*ln*1), where $x = ln(\Delta t)$; (ii) a double logarithmic transformation (T*ln*2), where $x = ln[ln(\Delta t)]$; and (iii) a triple logarithmic transformation (T*ln*3), where $x = ln\{ln[ln(\Delta t)]\}$. This procedure was

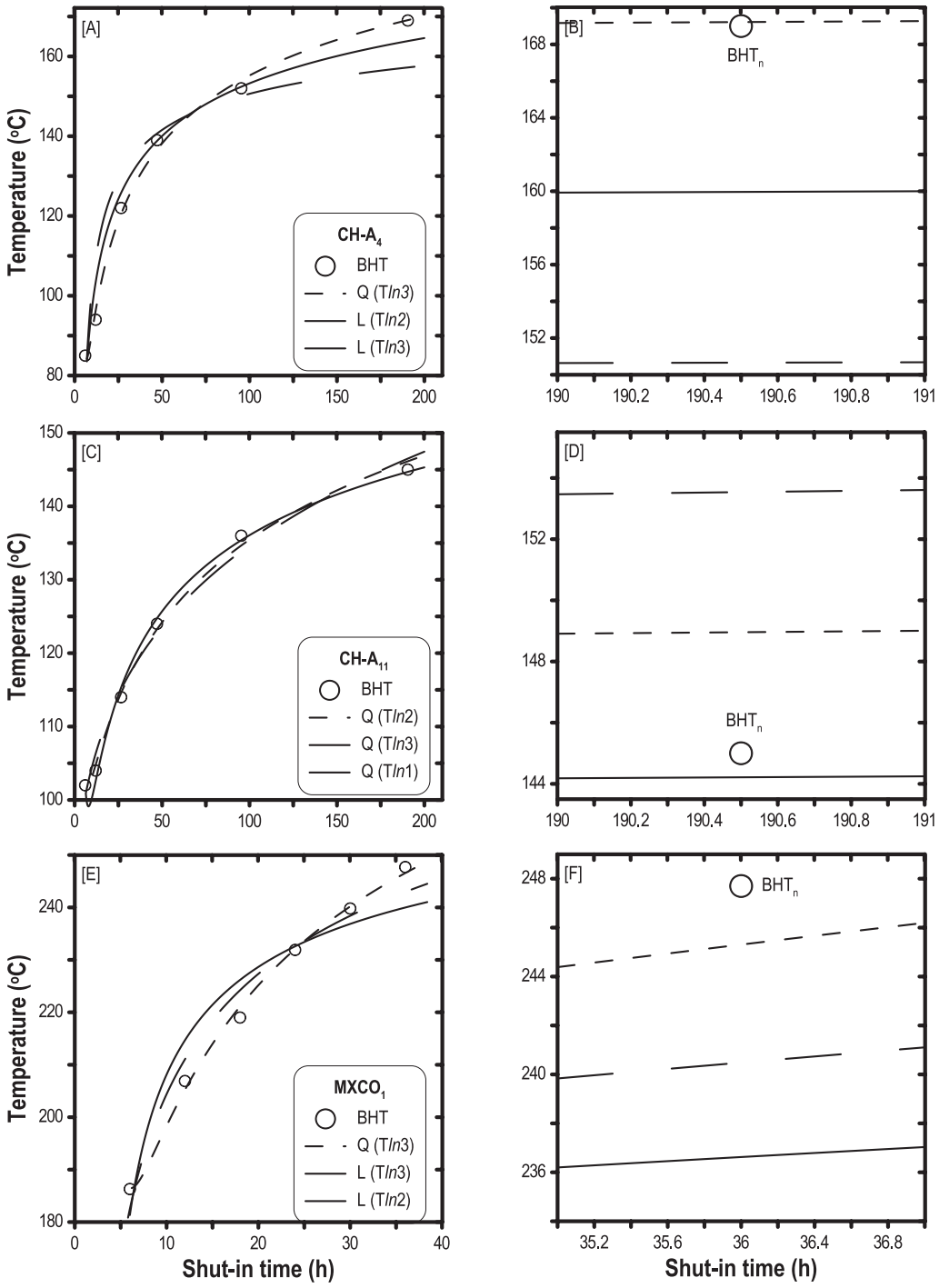

Figure 3. Integrated numerical simulation used for the regression models applied to geothermal data sets (A) CH-A_4, (C) CH-A_{11}, and (E) $MXCO_1$. BHT_n and numerical approximation plots obtained for the Ext-Abs parameter analysis: (B) CH-A_4; (D) CH-A_{11}; and (F) $MXCO_1$.

used to perform all the regression models to be involved in the GRM with the three described T*ln* transformations for each study case.

4.3. Applicability criterion

With the applicability criterion ($m \leqslant (n-1)/2$) it was possible to determine the maximum order of the GRM (equation (1)), and therefore, the different regression models used to calculate the SFT. The criterion consists of calculating the parameter m, which indicates the maximum order of the GRM to be used for each logarithmic transformation (T*ln*1; T*ln*2; T*ln*3) by using the number of measurements n as reference data. For instance (from table 1), for the CH-A_9 data set, which has six measurement data ($n = 6$), the applicability criterion will be equal to $m \leqslant 2.5$. The calculated value of m means that the maximum order of the GRM will be a QR model (i.e. a polynomial order of 2). In this particular case, only two different regression models, linear (L) and quadratic (Q), will be used for the determination of the SFT using each of the

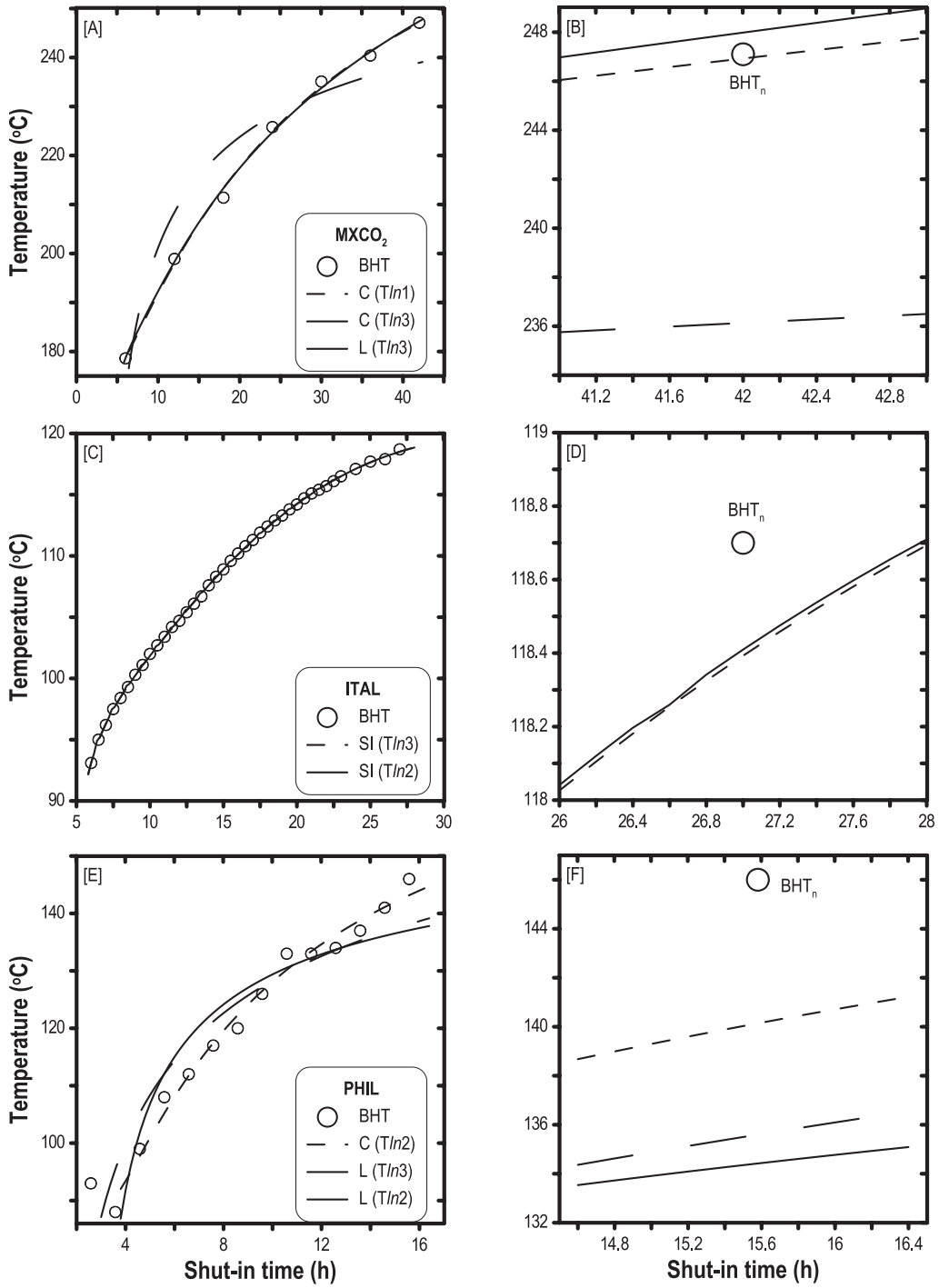

Figure 4. Integrated numerical simulation used for the regression models applied to geothermal data sets (A) $MXCO_2$, (C) ITAL, and (E) PHIL. BHT_n and numerical approximation plots obtained for the Ext-Abs parameter analysis: (B) $MXCO_2$; (D) ITAL; and (F) PHIL.

three log-transformations applied to the shut-in time measurements (i.e. T*ln*1; T*ln*2; and T*ln*3). Table 1 also includes the maximum orders of the polynomial regression models calculated for each recorded data set (according to the number of measurements reported).

4.4. Calculation of GRM coefficients

Once the maximum order of the polynomial regression models from each data set was determined (table 1), the regression coefficients of the GRM were calculated by applying the corresponding numerical algorithms of each regression model (linear or polynomial), and using the dependent (BHT) and independent (three T*ln*1; T*ln*2; and T*ln*3) variables for each data set (geothermal, petroleum, and permafrost). From the calculated coefficients of each regression model, the thermal behavior of the BHT was reproduced, and depending on the fitting quality, it could be used later to estimate the SFT by means of an extrapolation to infinite shut-in time.

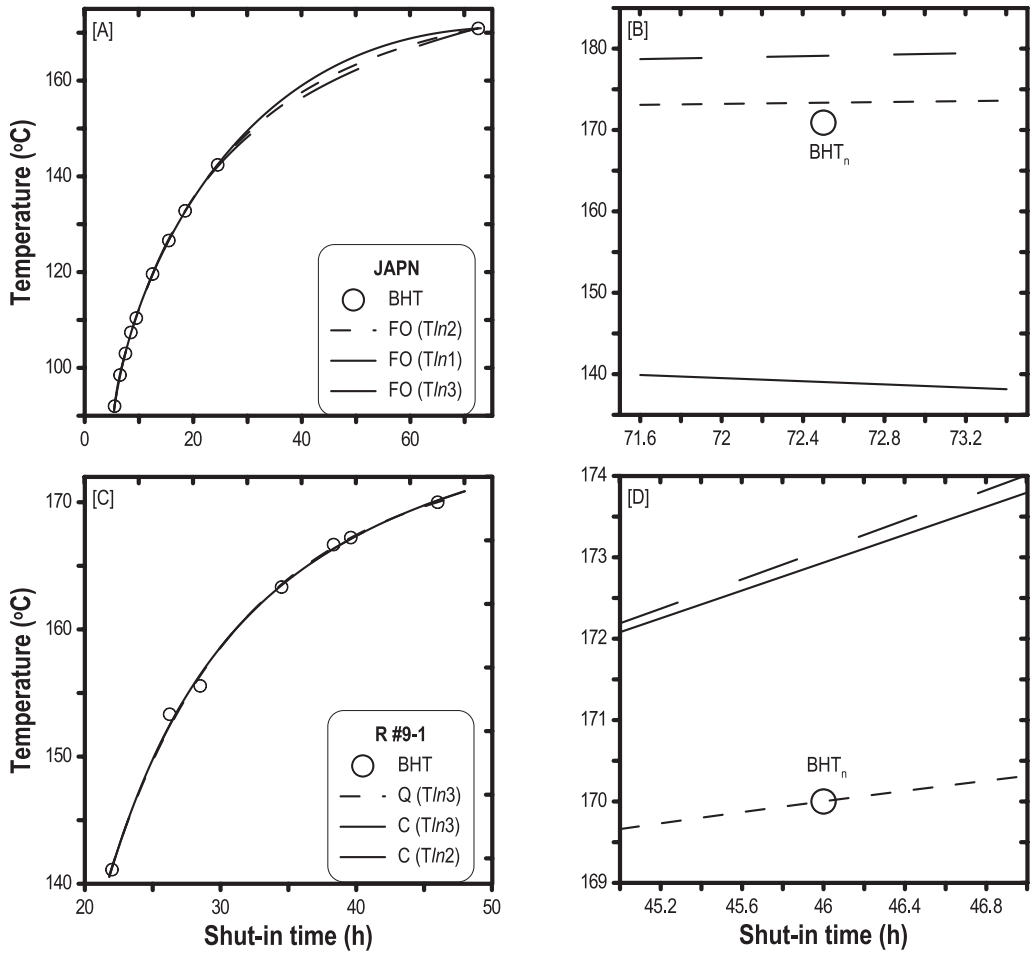

Figure 5. Integrated numerical simulation used for the regression models applied to geothermal data sets JAPN (A) and R #9-1 (C). BHT$_n$ and numerical approximation plots obtained for the Ext-Abs parameter analysis: (B) JAPN and (D) R #9-1.

For instance, with the same CH-A$_9$ data set ($n = 6$ and $m \leqslant 2.5$), it was inferred that the linear and quadratic regression models must be used for the estimation of the SFT. The resulting linear and polynomial regression equations (with their respective coefficients, a_i) were as follows:

(a) For the linear (L) and quadratic (Q) regression models of the GRM, and using the BHT (y) and T$ln1$ [$x = ln(\Delta t)$] data, the corresponding regression equations were as follows:

$$L(\mathrm{T}ln1) \Rightarrow y = 70.85 + 12.77x$$

$$Q(\mathrm{T}ln1) \Rightarrow y = 76.44 + 9.18x + 0.51x^2$$

(b) For the L and Q regression models of the GRM, and using the BHT (y) and T$ln2$ $\{x = ln[ln(\Delta t)]\}$ data, the corresponding regression equations were as follows:

$$L(\mathrm{T}ln2) \Rightarrow y = 67.51 + 40.38x$$

$$Q(\mathrm{T}ln2) \Rightarrow y = 97.21 - 19.32x + 26.66x^2$$

(c) For the L and Q regression models of the GRM, and using the BHT (y) and T$ln3$: $x = ln\{ln[ln(\Delta t)]\}$ data, the corresponding regression equations were as follows:

$$L(\mathrm{T}ln3) \Rightarrow y = 110.95 + 39.83x$$

$$Q(\mathrm{T}ln3) \Rightarrow y = 103.84 + 41.87x + 48.54x^2$$

Finally, the log-transformation method theoretically assumes that from these individual regression equations, the original measurement data sets may be reliably reproduced (i.e. the thermal behavior) and therefore, the SFT can be predicted at infinite shut-in time (by an extrapolation of the thermal recovery curve). This example allows the numerical methodology to be described for the individual and systematic analysis of all the thermal histories logged for all the geothermal, petroleum and permafrost boreholes (included in table 1).

4.5. Selection of the 'best' GRM to reproduce transient temperature data (BHT) and calculation of SFT at infinite time ($\Delta t \rightarrow \infty$)

Upon obtaining the regression equations (GRM with Tln) for each data set (equation (1)), we proceeded to evaluate them statistically through the application of the evaluation criteria, which will define the 'best' regression model that will be used to determine the SFT of the boreholes under study. With these evaluation purposes and using the same CH-A$_9$ data set (as an example) and a rigorous value of %Dev $\leqslant 0.01$ for the

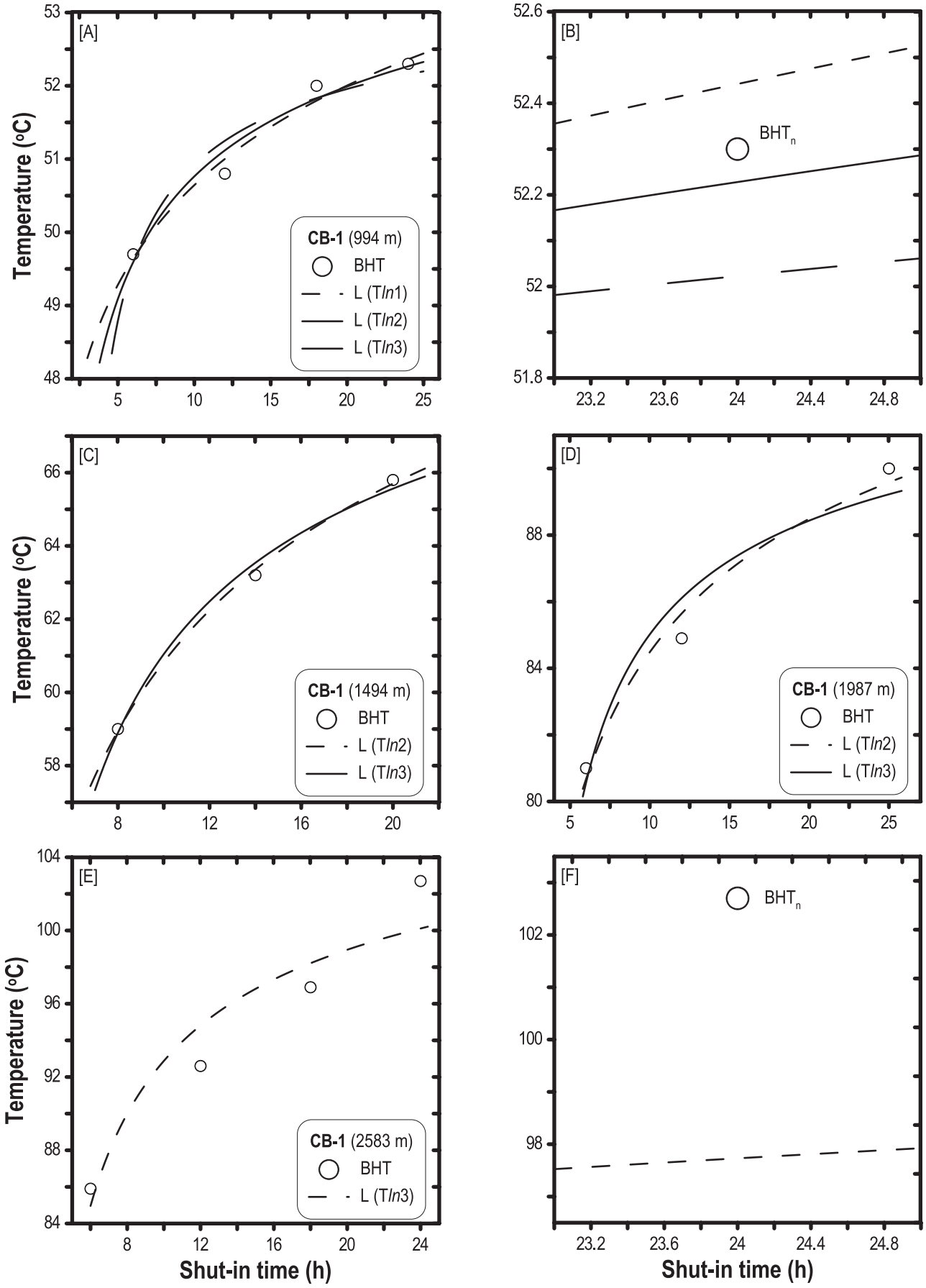

Figure 6. Integrated numerical simulation used for the regression models applied to geothermal data set CB-1: (A) 994 m; (C) 1494 m; (D) 1987 m; and (E) 2583 m. BHT$_n$ and numerical approximation plots obtained for the Ext-Abs parameter analysis: (B) 994 m and (D) 2583 m.

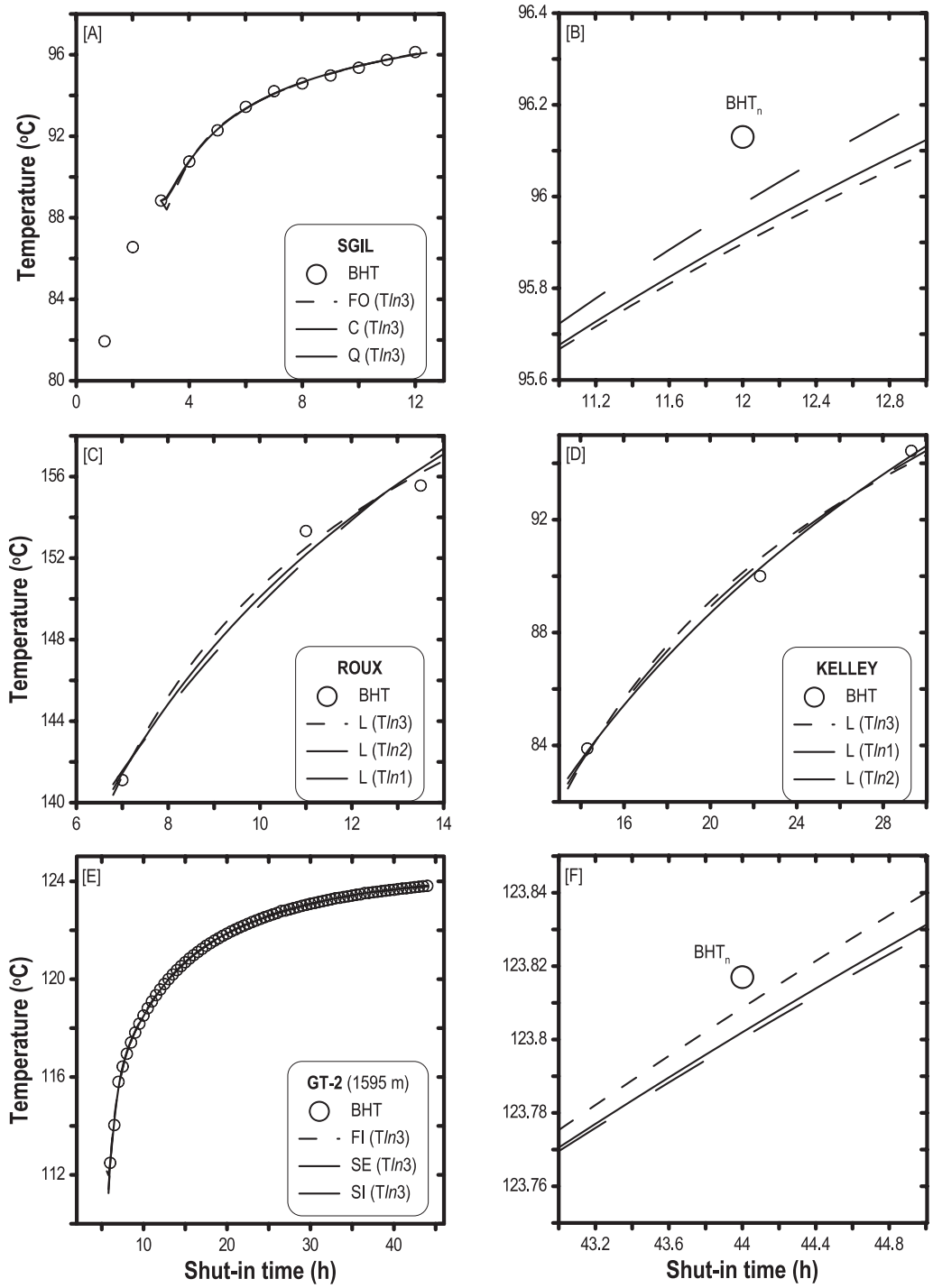

Figure 7. Integrated numerical simulation used for the regression models applied to geothermal data sets (A) SGIL, (C) ROUX (1518 m), (D) KELLEY (1035 m), and (E) GT-2 (1595 m), using the GRM with T*ln*. BHT$_n$ and numerical approximation plots obtained for the Ext-Abs parameter analysis: (B) SGIL and (F) GT-2 (1595 m).

numerical simulation, the statistical parameters R^2, RSSn, Ext-Abs and %Dev were calculated (table 2).

From a general view, it was observed that the quadratic models with T*ln* {Q(T*ln*1); Q(T*ln*2); and Q(T*ln*3)} have systematically much better values of R^2 and lower residuals (RSSn) than the linear models. In this way, the quadratic models fulfill enough of the two first two statistical criteria established by the parameters R^2 and RSSn, which is confirmed by observing the thermal behaviors plotted in figures 2(A), (C) and (E).

An additional evaluation parameter was also calculated by applying the third criterion (Ext-Abs) to all the regression models. With these purposes, the value of BHT$_n$ was determined by using the obtained regression equations {L(T*ln*1) and Q(T*ln*1); L(T*ln*2) and Q(T*ln*2); L(T*ln*3) and Q(T*ln*3)}. The resulting calculations were also shown in the plots of figures 2(B), (D) and (F).

The last selection criterion (referred to as deviation percentage: %Dev) was used as a dimensionless parameter for

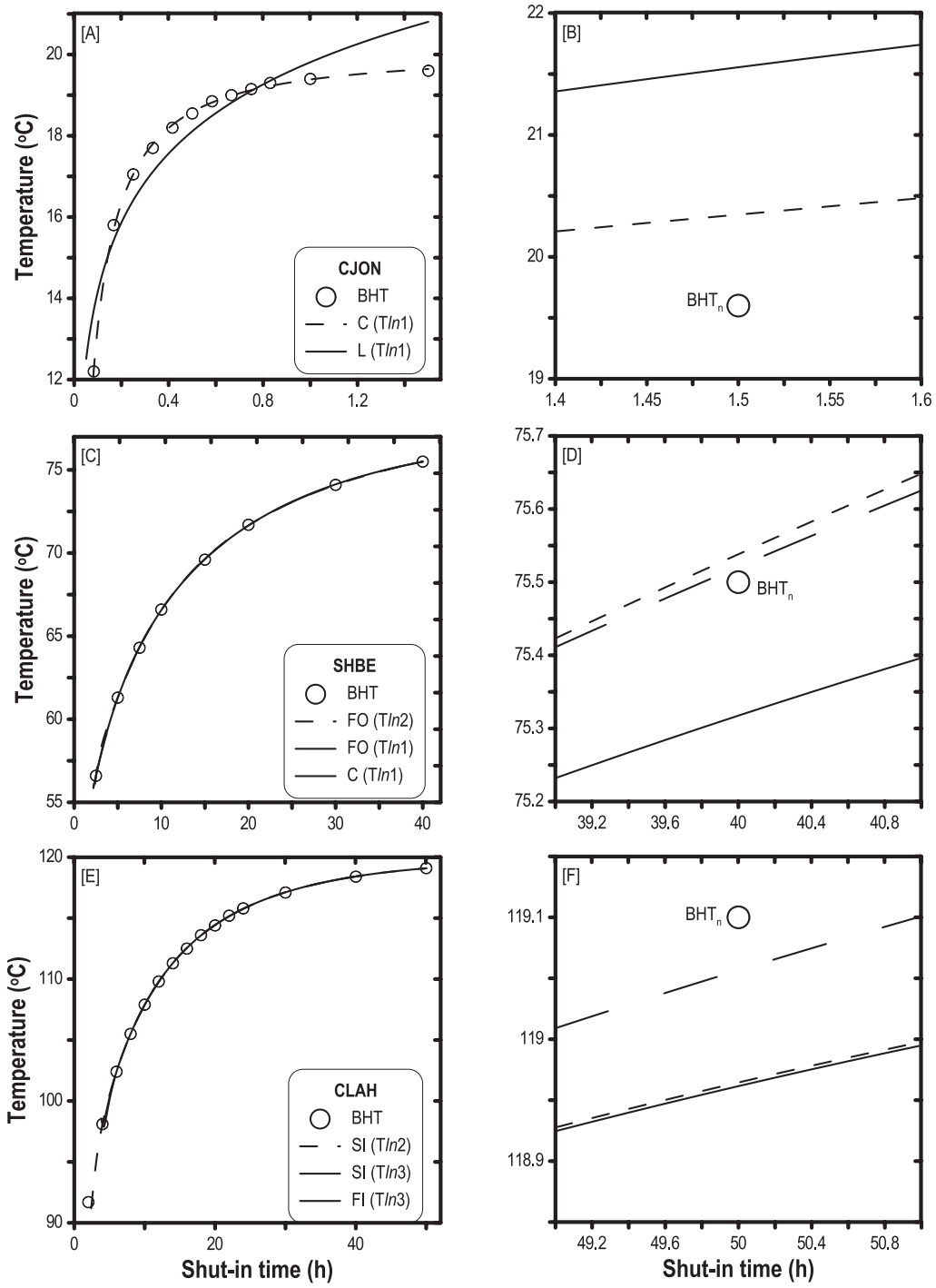

Figure 8. Integrated numerical simulation used for the regression models applied to synthetic data sets (A) CJON, (C) SHBE, and (E) CLAH, through the GRM with T*ln*. BHT$_n$ and numerical approximation plots obtained for the Ext-Abs parameter analysis: (B) CJON; (D) SHBE; and (F) CLAH.

the determination of the SFT by using a numerical simulation of the thermal recovery patterns predicted for each GRM (with T*ln*). With these purposes, the last BHT measurement logged (e.g. for the CH-A$_9$ data set: BHT$_n$ = 138 °C at a shut-in time of 190.5 h) was used both to assure that the GRM (with T*ln*) does not underestimate the SFT with regard to the last logged BHT$_n$ value and to calculate the SFT. For instance, given the magnitude of the geothermal borehole temperatures (logged for the CH-A$_9$), %Dev $\leqslant$ 0.01 was used as the convergence criterion of the numerical simulation for predicting the SFT (i.e. the numerical prediction must fulfill (SFT$_{n+1}$ − SFT$_n$)/SFT$_{n+1}$ $\leqslant$ 0.01).

For this particular case of analysis (CH-A$_9$), it was observed, in general, that in accordance with the increase of T*ln* level (from T*ln*1 to T*ln*3) in *L* regression models, the fitting quality of the BHT data decreases, whereas for the *Q* regression models a reverse behavior is obtained. However, as an exception case of the *L* regression model, it was observed

Table 5. A summary of the numerical results obtained for the application of the new method to the synthetic data sets CJON, SHBE and CLAH (using as rigorous value %Dev $\leqslant 0.01$ for the SFT numerical prediction).

Model	R^2	RSSn	Ext-Abs	SFT (°C)
CJON ($n = 12$, $BHT_n = 19.6$ °C, TFT = 20.25 °C)				
C (T*ln*1)	0.999 158	0.003 433	0.038 091	19.662 649
L (T*ln*1)	0.888 882	0.453 271	0.099 774	22.695 986
SHBE ($n = 8$, $BHT_n = 75.5$ °C, TFT = 80.0 °C)				
FO (T*ln*2)	0.999 98	0.000 757	0.000 505	78.176 02
FO (T*ln*1)	0.999 976	0.000 910	0.002 418	76.744 824
C (T*ln*1)	0.999 969	0.001 146	0.000 277	77.195 069
CLAH ($n = 15$, $BHT_n = 119.1$ °C, TFT = 120.0 °C)				
SI (T*ln*2)	0.999 989	0.000 622	0.001 137	119.566 18
SI (T*ln*3)	0.999 981	0.000 668	0.001 163	119.519 52
FI (T*ln*3)	0.999 981	0.000 679	0.000 365	119.578 56

Table 6. Summary of the obtained SFT estimations through the log-transformation (T*ln*) method using the geothermal and synthetic temperature data sets.

Data sets	BHT_n (°C)	Model T*ln*	SFT (°C)
Geothermal boreholes:			
CH-A_4	169	L (T*ln*2)	181 ± 2
CH-A_9	138	Q (T*ln*3)	148 ± 1
CH-A_{11}	145	Q (T*ln*3)	159 ± 2
$MXCO_1$	247.7	Q (T*ln*3)	320 ± 3
$MXCO_2$	247.1	C (T*ln*1)	275 ± 3
ITAL	118.7	SI (T*ln*3)	120 ± 1
PHIL	146	L (T*ln*3)	158 ± 2
JAPN	170.9	FO (T*ln*2)	176 ± 2
R #9-1	170	Q (T*ln*3)	173 ± 2
CB-1 (994 m)	52.3	L (T*ln*1)	58 ± 1
CB-1 (1494 m)	65.8	L (T*ln*2)	79 ± 1
CB-1 (1987 m)	90	L (T*ln*2)	98 ± 1
CB-1 (2583 m)	102.7	L (T*ln*3)	109 ± 1
SGIL	96.13	FO (T*ln*3)	102 ± 1
ROUX	155.56	L (T*ln*3)	180 ± 2
KELLEY	94.44	L (T*ln*3)	112 ± 1
GT-2 (1595 m)	123.817	SE (T*ln*3)	124 ± 1
Synthetic data:			
CJON	19.6	C (T*ln*1)	19.7 ± 0.2
SHBE	75.5	FO (T*ln*2)	78 ± 1
CLAH	119.1	SI (T*ln*2)	120 ± 1

that the predicted behavior by the regression model *L*(T*ln*1) provides a much better estimation of the extrapolated value of BHT_n in comparison with the other *L* or *Q* regression models (figure 2(B)). This result, even though seeming to contradict the previous evaluation results (see table 2), makes difficult the selection of the 'best' regression or fitting model. Therefore, a solid criterion of selection requires the largest number of evaluation criteria to come out for deciding the best regression model to finally determine the SFT.

With the integration of all these fundamental criteria and after analyzing all the results obtained for the thermal recovery

Table 7. A summary of the numerical results obtained for the application of the new method to the petroleum data sets COST, USAM, MALOOB, PPH-ABA and BECU (using as rigorous value %Dev $\leqslant 0.01$ for the SFT numerical prediction).

Model	R^2	RSSn	Ext-Abs	SFT (°C)
COST (1420 m) ($n = 6$, $BHT_n = 56.11$ °C)				
L (T*ln*3)	0.821 036	3.580 292	0.074 993	61.311 327
L (T*ln*2)	0.756 32	4.874 985	0.091 726	63.710 132
L (T*ln*1)	0.677 809	6.445 655	0.114 891	69.358 841
COST (3710 m) ($n = 5$, $BHT_n = 150$ °C)				
Q (T*ln*3)	0.984 304	2.423 206	0.032 93	165.724 55
Q (T*ln*2)	0.984 261	2.429 81	0.033 565	164.354 74
Q (T*ln*1)	0.983 694	2.517 377	0.034 948	153.060 21
COST (4475 m) ($n = 4$, $BHT_n = 174.44$ °C)				
L (T*ln*3)	0.956 214	0.830 434	0.004 879	188.1315
L (T*ln*2)	0.952 101	0.908 436	0.003 154	197.0859
L (T*ln*1)	0.945 707	1.029 703	0.004 879	220.199 27
USAM ($n = 14$, $BHT_n = 147.27$ °C)				
SI (T*ln*1)	0.999 999	0.000 004	0.000 003	149.204 34
SI (T*ln*2)	0.999 999	0.000 005	0.000 059	150.3086
SI (T*ln*3)	0.999 999	0.000 005	0.000 064	150.328 02
MALOOB—309D ($n = 7$, $BHT_n = 118$ °C)				
L (T*ln*3)	0.481 088	29.419 119	0.248 828	126.6137
L (T*ln*2)	0.470 75	30.005 256	0.2579	127.115 75
L (T*ln*1)	0.449 803	31.192 791	0.277 808	128.439 84
MALOOB—456 ($n = 9$, $BHT_n = 127$ °C)				
Q (T*ln*2)	0.948 886	22.285 757	14.168 513	139.768 06
Q (T*ln*3)	0.945 954	23.564 209	10.848 95	135.843 55
L (T*ln*2)	0.657 459	149.347 77	52.868 032	130.091 16
Franciacorta (3328 m) ($n = 4$, $BHT_n = 92$ °C)				
L (T*ln*1)	0.999 655	0.001 725	0.001 453	100.800 77
L (T*ln*2)	0.989 163	0.054 187	0.007 453	95.745 028
L (T*ln*3)	0.963 931	0.180 344	0.012 594	93.593 147
BECU ($n = 5$, $BHT_n = 72$ °C)				
L (T*ln*2)	0.962 76	0.297 923	0.016 895	86.050 726
L (T*ln*3)	0.931 861	0.545 114	0.023 003	78.950 547

behavior of the geothermal borehole CH-A_9 (table 2), it was determined that the 'best' regression model was the model *Q*(T*ln*2) because this model fulfilled, mostly, the evaluation criteria. Thus, the application of the model *Q*(T*ln*2) at infinite times allows the SFT of CH-A_9 to be determined as 157 ± 2 °C.

4.5.1. Application of the new method to analyze the thermal recovery process of geothermal boreholes. In a similar way to the previously described numerical methodology, the geothermal borehole data sets were systematically analyzed for reproducing the thermal recovery processes and the determination of their SFT (CH-A_4, CH-A_{11}, $MXCO_1$, $MXCO_2$, ITAL, PHIL, JAPN, R #9-1, CB-1, SGIL, ROUX, KELLEY and GT-2). With these purposes, the methodology uses the applicability criterion reported in table 1.

To save space in the manuscript, a summary of the results obtained from the application of this numerical methodology is presented. Table 3 summarizes the numerical results obtained for the data sets CH-A_4 (948 m), CH-A_{11} (2298 m), $MXCO_1$, $MXCO_2$, ITAL, PHIL, JAPN (700 m) and R #9-1 (1518 m). As we can observe in this table, the 'best' regression models

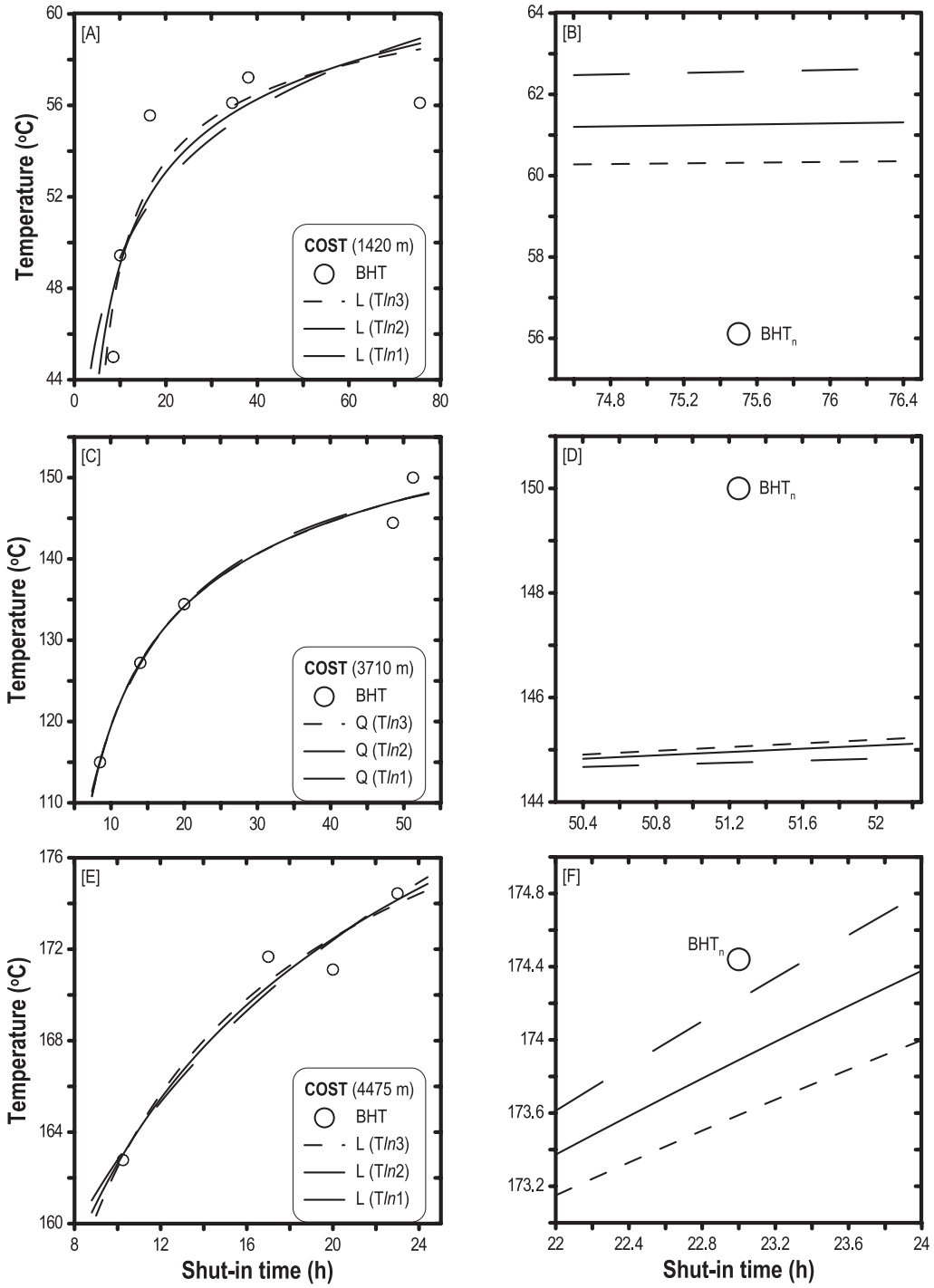

Figure 9. Integrated numerical simulation used for the GRM with T*ln* applied to the petroleum borehole COST: (A) 1420 m; (C) 3710 m; and (E) 4475 m. BHT$_n$ and numerical approximation plots obtained for the Ext-Abs parameter analysis: (B) 1420 m; (D) 3710 m; and (F) 4475 m.

that describe the thermal histories of the boreholes CH-A$_4$, CH-A$_{11}$, MXCO$_1$, MXCO$_2$, ITAL, PHIL, JAPN and R #9-1 were Q(T*ln*3), Q(T*ln*2), Q(T*ln*3), C(T*ln*1), SI(T*ln*3), C(T*ln*2), FO(T*ln*2) and C(T*ln*3), respectively.

Table 4 summarizes the numerical results obtained for the analysis of the geothermal data sets CB-1, SGIL, ROUX, KELLEY and GT-2, where we can observe that the 'best' fix models that describe the thermal recovery of the boreholes CB-1 (994 m), CB-1 (1494 m), CB-1 (1987 m), CB-1 (2583 m), SGIL, ROUX (1518 m) and KELLEY (1035 m) were L(T*ln*1), L(T*ln*2), L(T*ln*2), L(T*ln*3), FO(T*ln*3), L(T*ln*3) and L(T*ln*3), respectively. These results were represented and validated with the plots shown in figures 3–7, according to the following group distribution: figure 3 (CH-A$_4$ (948 m), CH-A$_{11}$ (2298 m), and MXCO$_1$); figure 4 (MXCO$_2$, ITAL, and PHIL); figure 5 (JAPN (700 m) and R #9-1 (1518 m)); figure 6 (CB-1 (994 m), CB-1 (1494m), CB-1 (1987m), and CB-1 (2583 m)); and figure 7 (SGIL, ROUX (1518 m), KELLEY (1035 m) and

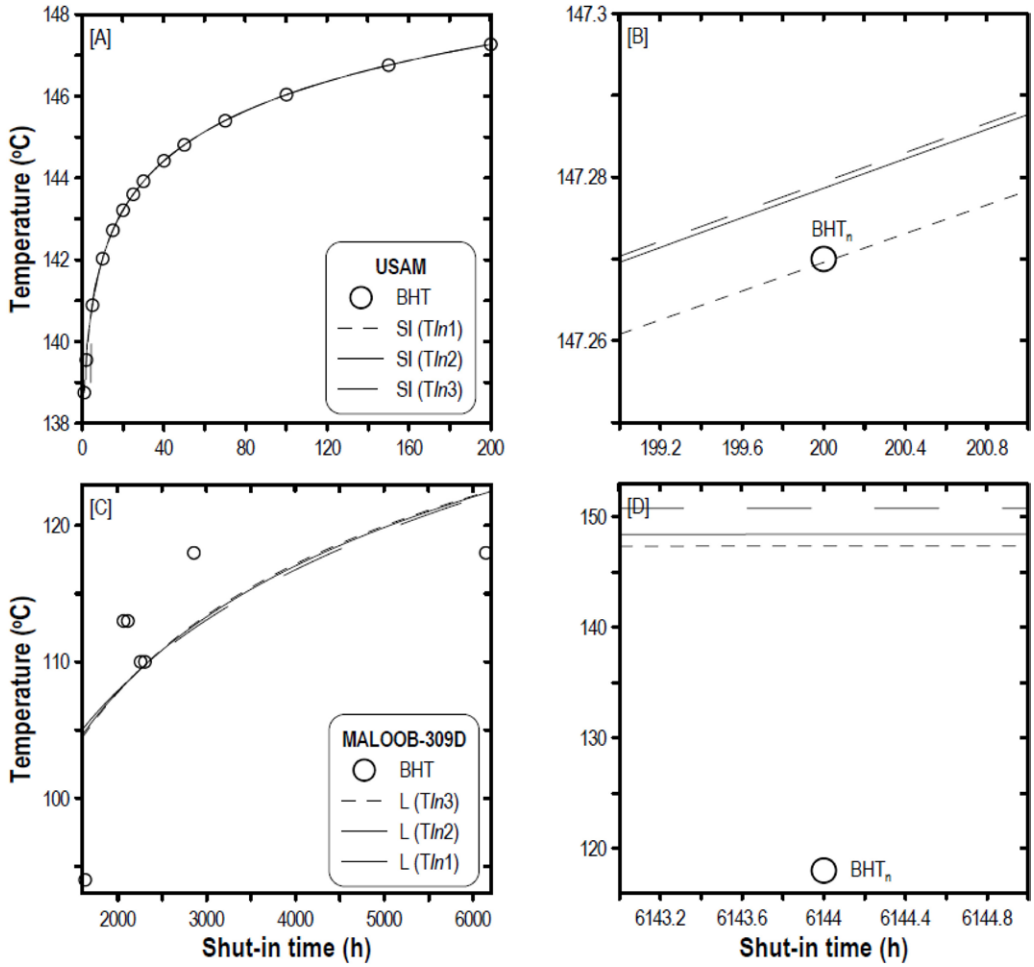

Figure 10. Integrated numerical simulation used for the GRM with T*ln* applied to the petroleum boreholes (A) USAM (4900 m) and (C) MALOOB-309D. BHT$_n$ and numerical approximation plots obtained for the Ext-Abs parameter analysis: (B) USAM (4900 m) and (D) MALOOB 309-D.

GT-2 (1595 m)). These plots include the BHT measurements, the numerical simulation of BHT through the T*ln* method and the extrapolation analysis (Ext-Abs) using a graphical zoom around the data reference BHT$_n$ (see figures 3(B), (D), (F), 4(B), (D), (F), 5(B), (D), 6(B), (F) and 7(B), (F)).

Thirty-nine BHT measurements were logged for the ITAL data set; therefore, the maximum order (EI) was achieved for the GRM. However, only two GRM models satisfied the established conditions in the four evaluation criteria.

For the data set PHIL's case, it was possible to apply the GRM of the sixth degree; therefore, numerical results with a variety of models were obtained. In the case of the JAPN and R#9-1 data sets, it was found that the three 'best' fix models were consistently polynomial models.

On the other hand, the geothermal data sets CB-1, ROUX and KELLEY showed a few BHT measurements ($n \leqslant 5$). Thus, in these examples it was just possible to apply the linear models with T*ln*. In the corresponding data sets of CB-1 (1494 m), CB-1 (1987 m), ROUX (1518 m) and KELLEY (1035 m), the criterion Ext-Abs was not applied due to its application requirements. As a consequence, only the obtained numerical results of the criteria R^2, RSSn and %Dev were analyzed. This showed a limitation of the new method, because only linear models can be applied.

Table 8. SFT estimations for the petroleum data sets, by means of the application of the T*ln* method.

Data sets	BHT$_n$ (°C)	Model T*ln*	SFT (°C)
Petroleum boreholes:			
USAM (4900 m)	147.27	SI (T*ln*1)	149.2 ± 0.2
COST (1420 m)	56.11	L (T*ln*3)	61 ± 1
COST (3710 m)	150	Q (T*ln*3)	166 ± 2
COST (4475 m)	174.44	L (T*ln*3)	188 ± 2
MALOOB—456	127	Q (T*ln*2)	140 ± 1
MALOOB—309D	118	L (T*ln*3)	127 ± 1
Franciacorta (3328 m)	92	L (T*ln*1)	101 ± 1
BECU (2700 m)	72	L (T*ln*2)	86 ± 1

The data set GT-2 (1595 m) is an example that has not been commonly reported in international literature, due its numerous BHT measurements ($n = 77$). Therefore, it becomes an ideal case for the application of the new method or for any thermal recovery analysis on geothermal boreholes.

From the results shown in table 4, it can be observed, almost consistently, the linear models prevail as the 'best' regression models, and consequently they have been suggested as

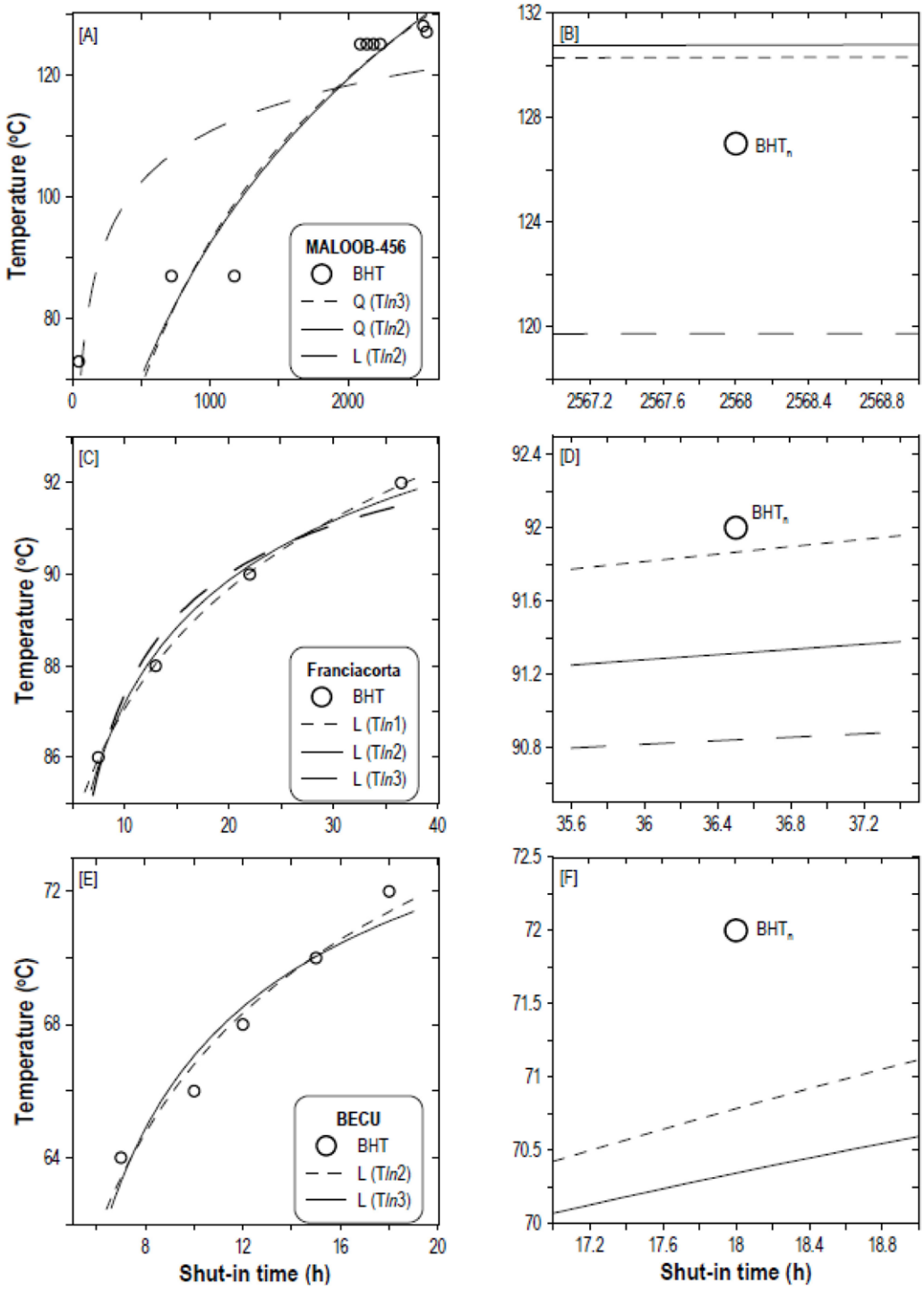

Figure 11. Integrated numerical simulation used for the GRM with T*ln* applied to the petroleum boreholes (A) MALOOB-456, (C) Franciacorta (3328 m), and (E) BECU (2700 m). BHT$_n$ and numerical approximation plots obtained for the Ext-Abs parameter analysis: (B) MALOOB-456; (D) Franciacorta (3328 m); and (F) BECU (2700 m).

the tools to estimate the SFT whereas some exceptions were found in the case of the KELLEY and GT-2 results where the polynomial models provide the 'best' regression models to obtain the SFT.

4.5.2. Application of the new method to analyze the thermal recovery process of synthetic datasets. Table 5 summarizes the numerical results obtained for the synthetic data sets CJON, SHBE and CLAH, whereas the predicted thermal recovery processes are shown in figure 8. The CJON data set was selected because it deals with data that correspond to low BHT and relatively shorter recovery times ($\Delta t \leqslant 1.5$ h). This example was very useful to verify the efficiency of the new method applied to this kind of synthetic BHT data. On the other hand, the SHBE data set was selected as a good example of medium BHT measurements, whereas the BHT measurements of the

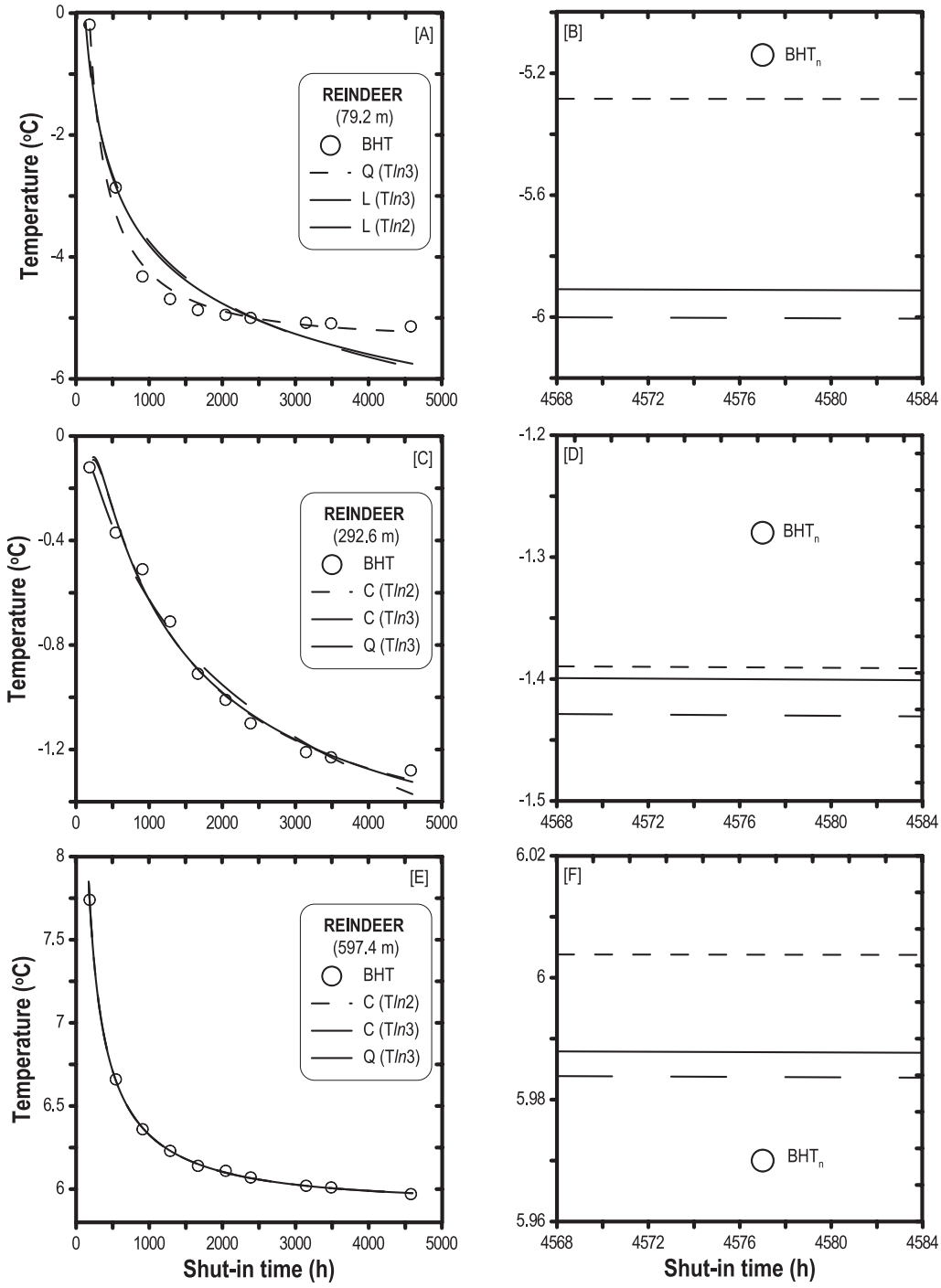

Figure 12. Integrated numerical simulation used for the regression models applied to the permafrost borehole REINDEER data: (A) (79.2 m); (C) (292.6 m); and (E) (597.4 m). BHT$_n$ and numerical approximation plots obtained for the Ext-Abs parameter analysis: (B) (79.2 m); (D) (292.6 m); and (F) (597.4 m).

CLAH data set enabled us to represent a typical case of a geothermal borehole with relatively high temperature.

From the numerical results reported in table 5, it can be observed in the case of CJON analysis that only two models fulfilled the requirements of the evaluation criteria, and the calculation of SFT was through the application of a polynomial regression (C) model (T*ln*1). On the other hand, it was also found for the SHBE and CLAH synthetic data sets that the fourth and sixth polynomial regression models with T*ln*2 were the best fitting models, respectively.

Finally, table 6 shows the SFTs and their uncertainties calculated for each geothermal and synthetic data set, inferred by means of the GRM (with T*ln*). The BHT$_n$ from each data set are included as additional data with the purpose of demonstrating that the ideal GRM (with T*ln*) does not underestimate the SFT.

4.5.3. Application of the new method to analyze the thermal recovery process of petroleum boreholes. Table 7 presents the obtained numerical results for the petroleum data sets

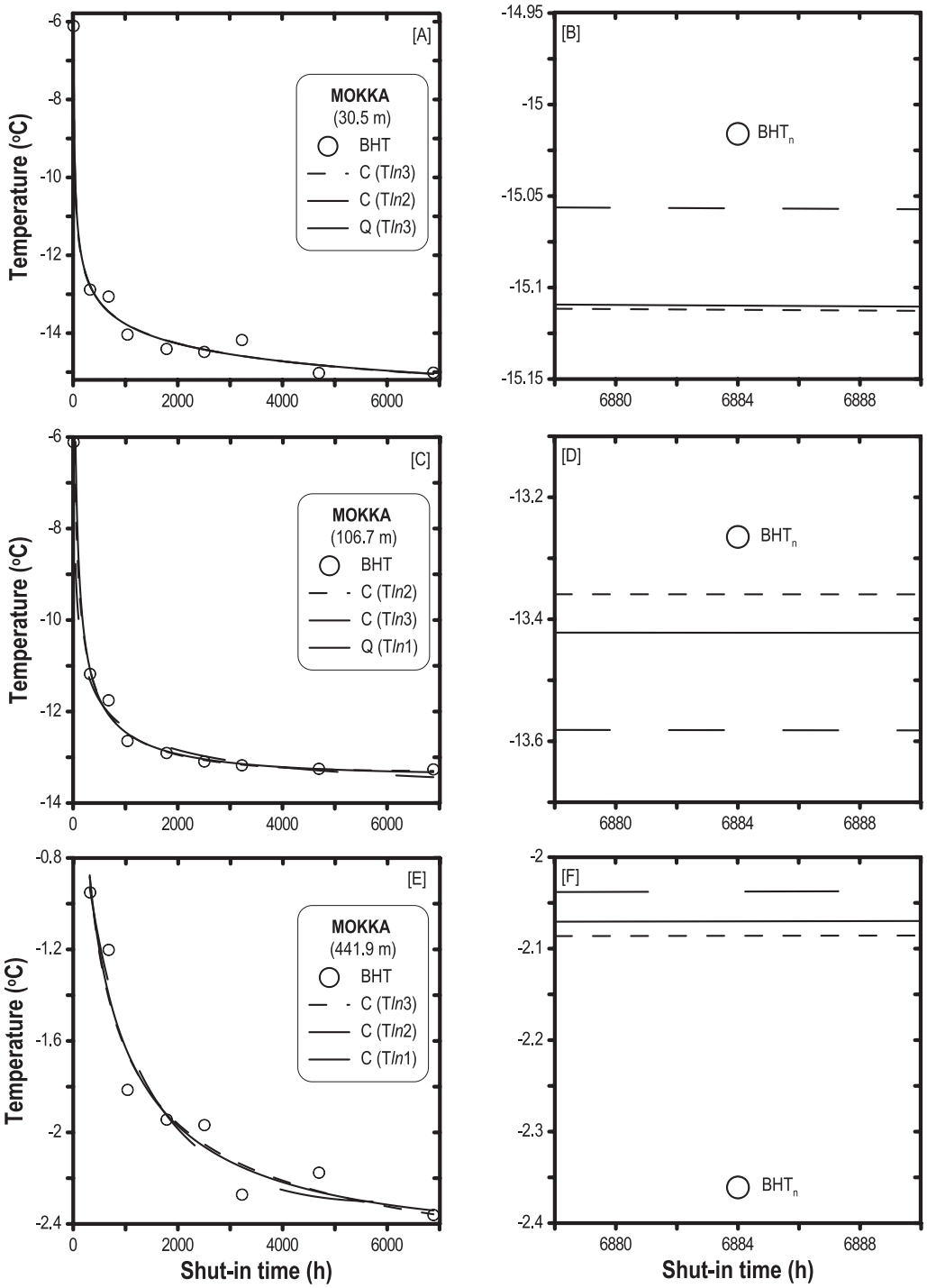

Figure 13. Integrated numerical simulation used for the regression models applied to the permafrost borehole MOKKA data: (A) (30.5 m); (C) (106.7 m); and (E) (441.9 m). BHT$_n$ and numerical approximation plots obtained for the Ext-Abs parameter analysis: (B) (30.5 m); (D) (106.7 m); and (F) (441.9 m).

USAM (4900 m), COST, MALOOB, PPH-ABA and BECU (2700 m). The data group COST consists of three logged data sets at different depths and temperature ranges of thermal recovery. In the petroleum case MALOOB, the data sets MALOOB-456 and MALOOB-309D were used, while for the case PPH-ABA, the data set Franciacorta (3328 m) was used. Figures 9(A), (C) and (E) show the measured BHT data from COST (1420 m), COST (3710 m) and COST (4475 m), and the obtained results from the numerical simulations. Furthermore, the plots of figures 9(B), (D) and (F) correspond to the graphical representation of the Ext-Abs criterion numerical results. Finally, the BHT data from the petroleum boreholes USAM, MALOOB, PPH-ABA and BECU, as well as the BHT numerical reproduction by means of the GRM (T*ln*) models' computer simulation and the respective extrapolation analysis (Ext-Abs), are shown in figures 10 and 11.

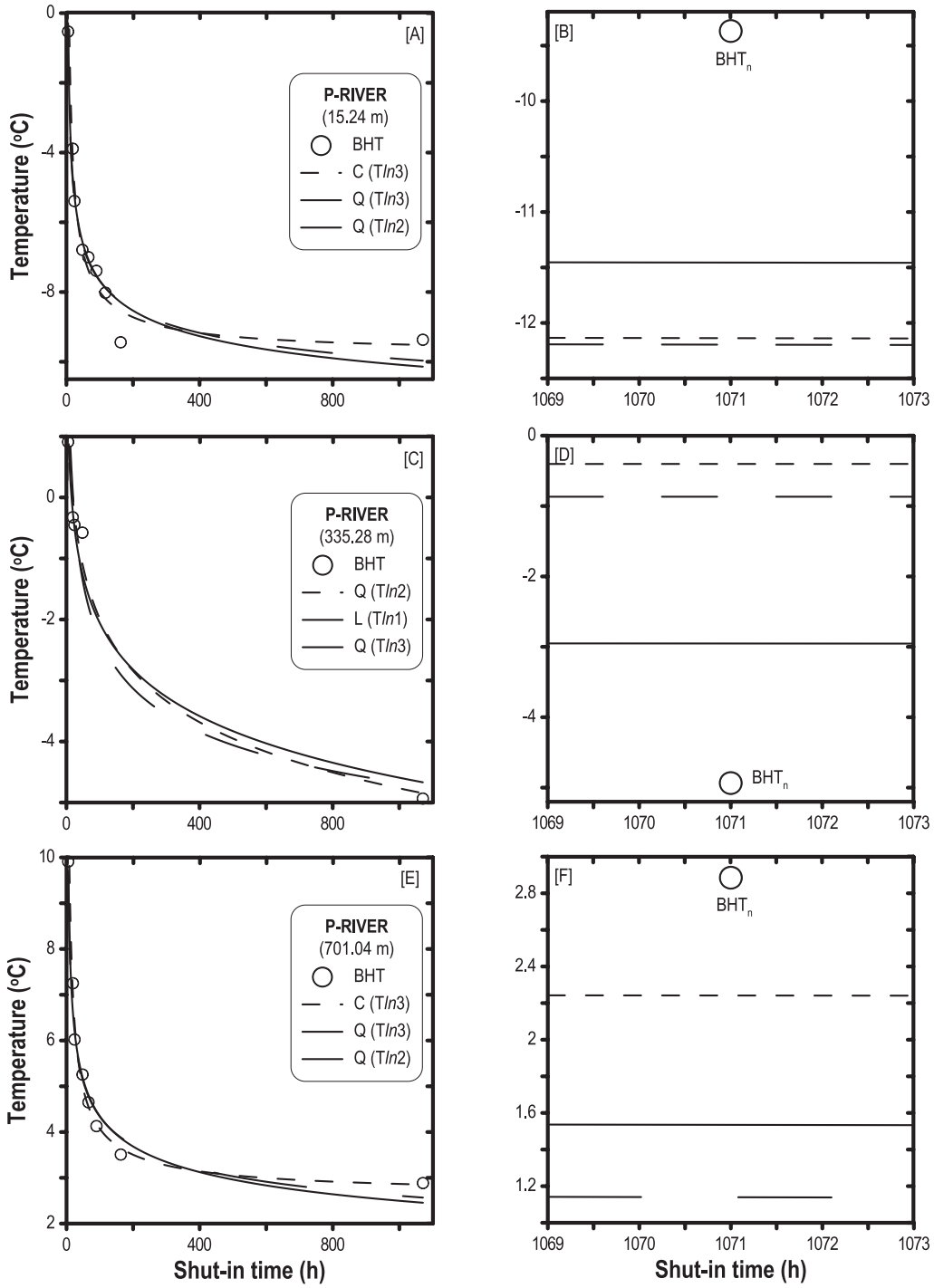

Figure 14. Integrated numerical simulation used for the regression models applied to the permafrost borehole P-RIVER data: (A) (15.24 m); (C) (335.28 m); and (E) (701.04 m). BHT$_n$ and numerical approximation plots obtained for the Ext-Abs parameter analysis: (B) (15.24 m); (D) (335.28 m); and (F) (701.04 m).

In a general way and in relation to the obtained numerical results from the petroleum boreholes COST (1420 m), COST (3710 m), COST (4475 m), MALOOB-456, MALOOB-309D, Franciacorta (3328 m) and BECU (2700 m), the best fix models were *L*(T*ln*3), *Q*(T*ln*3), *L*(T*ln*3), *Q*(T*ln*2), *L*(T*ln*3), *L*(T*ln*1) and *L*(T*ln*2), respectively. In the particular case of the data set USAM (table 7 and figure 10), it can be observed that there is practically no existence of numerical difference between the predictions carried out by the three 'best' fix models (SI(T*ln*1), SI(T*ln*2) and SI(T*ln*3)), as what happens in a lot of geothermal cases.

Table 8 shows a summary of the calculated SFTs and their respective uncertainties for each petroleum data set analyzed with the selected GRM (T*ln*) models.

4.5.4. Application of the new method to the analysis of the thermal recovery process of permafrost boreholes. In a similar way to the previously described numerical methodology, the

Table 9. A summary of the numerical results obtained for the application of the new method to the permafrost data borehole REINDEER (using as rigorous value %Dev ⩽ 0.001 for the SFT numerical prediction).

Model	R^2	RSSn	Ext-Abs	SFT (°C)
REINDEER (18.3 m) ($n = 9$, $BHT_n = -7.69$ °C)				
L (T*ln*3)	0.944 148	0.233 615	0.021 614	−9.117 11
L (T*ln*2)	0.929 968	0.292 926	0.005 69	−9.629 47
L (T*ln*1)	0.895 713	0.436 205	0.025 361	−10.931 07
REINDEER (48.8 m) ($n = 9$, $BHT_n = -5.58$ °C)				
C (T*ln*3)	0.999 958	0.000 113	0.009 629	−5.664 63
C (T*ln*2)	0.999 934	0.000 176	0.012 824	−6.026 79
C (T*ln*1)	0.999 812	0.000 503	0.023 539	−12.4364
REINDEER (79.2 m) ($n = 10$, $BHT_n = -5.14$ °C)				
Q (T*ln*3)	0.987 126	0.028 617	0.028 054	−5.249 55
L (T*ln*3)	0.925 19	0.166 289	0.149 964	−6.836 49
L (T*ln*2)	0.904 862	0.211 473	0.167 925	−7.175 05
REINDEER (140.2 m) ($n = 10$, $BHT_n = -4.3$ °C)				
Q (T*ln*1)	0.958 276	0.073 738	0.117 861	−5.700 82
Q (T*ln*3)	0.957 635	0.074 87	0.129 196	−6.192 97
Q (T*ln*2)	0.956 732	0.076 466	0.12 805	−6.161 24
REINDEER (201.2 m) ($n = 10$, $BHT_n = -3.11$ °C)				
Q (T*ln*1)	0.997 466	0.001 624	0.000 612	−3.112 16
Q (T*ln*2)	0.994 872	0.003 288	0.022 786	−3.188 08
Q (T*ln*3)	0.993 422	0.004 217	0.031 296	−3.258 95
REINDEER (292.6 m) ($n = 10$, $BHT_n = -1.28$ °C)				
C (T*ln*2)	0.990 826	0.001 329	0.086 32	−1.455 95
C (T*ln*3)	0.989 779	0.001 481	0.093 912	−1.561 14
Q (T*ln*3)	0.983 646	0.002 369	0.117 03	−2.204 25
REINDEER (414.5 m) ($n = 10$, $BHT_n = 1.25$ °C)				
C (T*ln*2)	0.999 969	0.000 011	0.001 253	1.215 17
FO (T*ln*1)	0.999 973	0.000 009	0.016 733	1.194 65
C (T*ln*1)	0.999 967	0.000 011	0.011 554	−0.785 04
REINDEER (506 m) ($n = 10$, $BHT_n = 3.49$ °C)				
FO (T*ln*1)	0.999 971	0.000 009	0.000 119	3.472 45
C (T*ln*2)	0.999 967	0.000 01	0.001 036	3.475 19
REINDEER (597.4 m) ($n = 10$, $BHT_n = 5.97$ °C)				
C (T*ln*2)	0.999 853	0.000 038	0.002 746	5.9448
C (T*ln*3)	0.999 841	0.000 041	0.002 979	5.9529
Q (T*ln*3)	0.999 835	0.000 043	0.002 297	5.959 66

Table 10. A summary of the numerical results obtained for the application of the new method to the permafrost data borehole MOKKA (using as rigorous value %Dev ⩽ 0.001 for the SFT numerical prediction).

Model	R^2	RSSn	Ext-Abs	SFT (°C)
MOKKA (15.2 m) ($n = 6$, $BHT_n = -15.371$ °C)				
Q (T*ln*2)	0.998 955	0.015 957	0.006 378	−15.499 38
Q (T*ln*1)	0.998 944	0.016 138	0.014 344	−15.392 82
L (T*ln*3)	0.998 929	0.016 363	0.001 092	−15.378 63
MOKKA (30.5 m) ($n = 9$, $BHT_n = -15.016$ °C)				
C (T*ln*3)	0.992 194	0.053 543	0.006 403	−15.116 95
C (T*ln*2)	0.992 187	0.053 593	0.006 250	−15.104 76
Q (T*ln*3)	0.992 186	0.053 596	0.002 711	−15.085 16
MOKKA (45.7 m) ($n = 9$, $BHT_n = -14.629$ °C)				
C (T*ln*1)	0.998 453	0.006 363	0.005 049	−14.716 63
Q (T*ln*1)	0.998 269	0.007 118	0.007 963	−14.929 27
C (T*ln*2)	0.998 257	0.007 169	0.008 639	−14.883 71
MOKKA (61 m) ($n = 7$, $BHT_n = -14.304$ °C)				
C (T*ln*2)	0.997 490	0.011 827	0.013 306	−14.386 77
Q (T*ln*1)	0.995 861	0.019 499	0.022 153	−14.558 68
Q (T*ln*2)	0.994 532	0.025 76	0.026 75	−14.829 09
MOKKA (76.2 m) ($n = 9$, $BHT_n = -14.083$ °C)				
C (T*ln*2)	0.993 874	0.026 332	0.007 205	−14.126 19
C (T*ln*3)	0.993 392	0.028 402	0.011 565	−14.191 20
Q (T*ln*1)	0.992 369	0.032 802	0.018 473	−14.388 44
MOKKA (91.4 m) ($n = 8$, $BHT_n = -13.808$ °C)				
Q (T*ln*1)	0.996 520	0.018 257	0.013 921	−13.970 35
Q (T*ln*2)	0.992 879	0.037 363	0.027 100	−14.046 11
Q (T*ln*3)	0.992 823	0.037 654	0.027 821	−14.083 75
MOKKA (106.7 m) ($n = 9$, $BHT_n = -13.265$ °C)				
C (T*ln*2)	0.996 978	0.014 221	0.034 122	−13.298 17
C (T*ln*3)	0.996 577	0.016 105	0.011 845	−13.338 79
Q (T*ln*1)	0.994 549	0.025 648	0.023 884	−13.610 69
MOKKA (152.4 m) ($n = 7$, $BHT_n = -11.277$ °C)				
C (T*ln*1)	0.996 042	0.011 100	0.003 741	−11.363 62
C (T*ln*2)	0.995 957	0.011 338	0.000 530	−11.292 62
C (T*ln*3)	0.995 937	0.011 394	0.001 889	−11.594 63
MOKKA (198.1 m) ($n = 8$, $BHT_n = -9.32$ °C)				
Q (T*ln*1)	0.963 645	0.062 832	0.085 784	−9.847 98
Q (T*ln*3)	0.962 290	0.065 174	0.083 807	−10.054 34
Q (T*ln*2)	0.960 462	0.068 333	0.086 776	−10.069 75
MOKKA (320 m) ($n = 7$, $BHT_n = -6.906$ °C)				
C (T*ln*3)	0.997 157	0.001 604	0.016 952	−7.499 04
C (T*ln*2)	0.996 862	0.001 771	0.019 815	−7.350 62
C (T*ln*1)	0.994 900	0.002 878	0.030 533	−6.989 53
MOKKA (441.9 m) ($n = 9$, $BHT_n = -2.361$ °C)				
Q (T*ln*1)	0.943 364	0.012 715	0.019 642	−2.403 88
Q (T*ln*2)	0.941 163	0.013 210	0.000 115	−2.429 55
Q (T*ln*3)	0.940 259	0.013 412	0.006 898	−2.460 57

permafrost borehole data sets were systematically analyzed for reproducing the thermal recovery processes and the determination of their SFT. Tables 9–11 and figures 12–14 show the numerical and graphical results for each data set of the permafrost boreholes REINDEER, MOKKA and P-RIVER, which received the same treatment of the last examples. The three 'best' fix models are listed, but for space limitations, only some of them are shown in figures 12(A), (C), (E), 13(A), (C), (E) and 14(A), (C), (E). The graphic amplification of the obtained numerical approximations of the GRM (T*ln*) models is shown in figures 12(B), (D), (F), 13(B), (D), (F) and 14(B), (D), (F). These permafrost exploration boreholes were selected to be analyzed due to their different ranges of 'cold' temperatures, around or less than 0 °C, and depths.

From table 9, only one linear model provided the best results in the first case (REINDEER 18.3 m), so this model was used to determine the SFT in the corresponding section. In the remaining sections (REINDEER) and the boreholes MOKKA (table 10) and P-RIVER (table 11), polynomial models were the 'best' fix models according to the evaluation criteria. In general, relevant discrepancies are not observed between the numerical predictions provided with each of the

Table 11. A summary of the numerical results obtained for the application of the new method to the permafrost data borehole P-RIVER (using as rigorous value %Dev ⩽ 0.001 for the SFT numerical prediction).

Model	R^2	RSSn	Ext-Abs	SFT (°C)
P-RIVER (15.24 m) ($n = 9$, $BHT_n = -9.369$ °C)				
C (T*ln*3)	0.977 025	0.163 278	0.295 452	−9.577 25
Q (T*ln*3)	0.957 816	0.299 796	0.222 731	−11.302 70
Q (T*ln*2)	0.957 187	0.304 265	0.301 706	−10.941 26
P-RIVER (30.48 m) ($n = 9$, $BHT_n = -9.167$ °C)				
FO (T*ln*3)	0.989 711	0.078 599	0.385 402	−9.257 49
FO (T*ln*2)	0.988 417	0.088 491	0.424 543	−9.234 46
Q (T*ln*3)	0.942 530	0.439 038	1.296 310	−11.666 43
P-RIVER (45.72 m) ($n = 9$, $BHT_n = -9.052$ °C)				
FO (T*ln*3)	0.988 655	0.090 420	76.752 338	−9.426 17
FO (T*ln*2)	0.986 400	0.108 393	254.789 827	−13.156 41
Q (T*ln*1)	0.946 489	0.426 489	20.487 645	−9.360 02
P-RIVER (60.96 m) ($n = 9$, $BHT_n = -8.957$ °C)				
FO (T*ln*3)	0.991 309	0.061 889	45.148 756	−9.234 93
FO (T*ln*2)	0.989 991	0.071 274	131.669 369	−10.927 99
Q (T*ln*3)	0.954 231	0.325 926	5.310 914	−11.086 51
P-RIVER (91.44 m) ($n = 9$, $BHT_n = -8.771$ °C)				
FO (T*ln*3)	0.988 684	0.087 261	53.101 663	−9.513 73
FO (T*ln*2)	0.986 072	0.107 401	169.442 480	−15.726 59
Q (T*ln*1)	0.931 838	0.525 597	25.027 252	−9.132 18
P-RIVER (152.4 m) ($n = 9$, $BHT_n = -8.124$ °C)				
C (T*ln*3)	0.978 598	0.157 363	16.835 435	−8.703 13
Q (T*ln*3)	0.944 509	0.408 021	8.286 078	−11.536 75
Q (T*ln*1)	0.908 429	0.673 308	75.034 554	−10.257 37
P-RIVER (304.81 m) ($n = 5$, $BHT_n = -5.462$ °C)				
Q (T*ln*2)	0.982 172	0.083 204	21.286 175	−8.537 79
Q (T*ln*3)	0.959 846	0.187 405	18.710 074	−7.019 35
L (T*ln*1)	0.959 032	0.191 202	6.580 069	−8.195 71
P-RIVER (335.28 m) ($n = 5$, $BHT_n = -4.935$ °C)				
Q (T*ln*2)	0.979 947	0.080 370	20.546 817	−7.632 48
L (T*ln*1)	0.967 906	0.128 630	3.930 330	−7.546 67
Q (T*ln*3)	0.958 627	0.165 820	16.542 837	−6.321 09
P-RIVER (396.24 m) ($n = 9$, $BHT_n = -4.039$ °C)				
FO (T*ln*3)	0.984 232	0.031 941	50.830 807	−4.241 41
C (T*ln*3)	0.967 932	0.064 958	8.825 567	−6.880 25
C (T*ln*2)	0.960 977	0.079 048	30.572 812	−7.626 70
P-RIVER (579.12 m) ($n = 9$, $BHT_n = -0.778$ °C)				
FO (T*ln*3)	0.998 885	0.000 985	0.866 575	−1.435 53
FO (T*ln*2)	0.998 834	0.001 030	2.153 146	−1.191 09
C (T*ln*2)	0.998 718	0.001 132	0.083 099	−1.876 62
P-RIVER (609.6 m) ($n = 9$, $BHT_n = -0.195$ °C)				
Q (T*ln*3)	0.909 995	0.090 411	2.007 245	−1.796 72
Q (T*ln*1)	0.878 840	0.121 707	11.443 311	−0.663 68
Q (T*ln*2)	0.865 085	0.135 524	4.941 936	−2.029 43
P-RIVER (640.08 m) ($n = 9$, $BHT_n = 0.761$ °C)				
Q (T*ln*1)	0.971 860	0.095 737	6.078 248	0.520 04
Q (T*ln*3)	0.964 014	0.122 429	2.139 353	−1.579 50
Q (T*ln*2)	0.952 984	0.159 955	4.881 918	−1.695 50
P-RIVER (670.56 m) ($n = 5$, $BHT_n = 1.664$ °C)				
Q (T*ln*2)	0.990 178	0.062 682	2.121 075	−0.018 68
Q (T*ln*3)	0.989 466	0.067 225	1.458 316	−0.235 47
L (T*ln*3)	0.975 693	0.155 114	0.597 726	1.142 11
P-RIVER (701.04 m) ($n = 8$, $BHT_n = 2.885$ °C)				
C (T*ln*3)	0.992 035	0.288 610	0.414 031	2.857 82
Q (T*ln*3)	0.975 785	0.109 671	1.822 725	−0.060 16
Q (T*ln*2)	0.975 421	0.111 319	3.046 635	1.190 55

analyzed models (figures 12, plots (C) and (E); figures 13, plots (A), (C) and (E)). Graphic–numerical discrepancies in the simulations are easier to detect in figures 12(A) and 14(A), (C), (E). Nevertheless, in the amplified plots from figures 12–14(B), (D) and (F), respectively, the emphasized differences between the results of the Ext-Abs criterion to each model can be observed; however, some of these results are not 'visible' in the numerical results of tables 9–11.

As of these last results, finally the SFTs were determined to each depth from the exploration permafrost boreholes REINDEER, MOKKA and P-RIVER, which are summarized in table 12.

After the analysis of all the cases of geothermal, petroleum and permafrost application, it is demonstrated that the coefficient of determination (R^2), the residuals normalized (RSSn), and the dimensional parameters of extrapolation and simulation convergence (Ext-Abs and %Dev, respectively) are fundamental for the evaluation of the regression models and log-transformation (T*ln*) applied together to each data set. These parameters are statistical criteria used to define the best fix model that describes the behavior of the BHT and shut-in time. This process has allowed us to indicate that each evaluation criterion is complementary to the others, a requirement that guarantees the effectiveness and reliability of the choice of the best models that will represent the analyzed temperature data sets with the new method.

After analyzing the results related to the best R^2, the lower residuals, and the most accurate numerical extrapolation and simulation (tables 2–5, 7 and 9–11), it is inferred systematically that the best fix models used together with the T*ln* of shut-in time were given by the achieved predictions with the polynomial models (e.g. Q(T*ln*1), Q(T*ln*2), Q(T*ln*3), …, EI(T*ln*1), EI(T*ln*2), EI(T*ln*3)). On and after the analysis of 17 geothermal temperature data sets, 8 were described through linear models (40%), while the remaining percentage were better analyzed by polynomial models (60%). In the eight petroleum cases, five were better represented by linear models (63%), than by the difference obtained with polynomial models (37%). Finally, in the analysis of the permafrost borehole data, only 1 of the 34 data sets was described by a linear model (3%) and the 97% were obtained successfully by polynomial models. In this way, and by doing a global analysis, it was found that from the 62 analyzed cases of thermal recovery, only 17 were described by linear models (27%) whereas 45 cases were better represented with non-linear models.

Table 12. Summary of the obtained SFT for the permafrost borehole data sets REINDEER, MOKKA, and P-RIVER, by the application of the T*ln* method.

Data sets	BHT_n (°C)	Model T*ln*	SFT (°C)
Permafrost borehole:			
REINDEER (18.3 m)	−7.69	L (T*ln*3)	−9.12 ± 0.01
REINDEER (48.8 m)	−5.58	C (T*ln*3)	−5.67 ± 0.01
REINDEER (79.2 m)	−5.14	Q (T*ln*3)	−5.25 ± 0.01
REINDEER (140.2 m)	−4.3	Q (T*ln*1)	−5.70 ± 0.01
REINDEER (201.2 m)	−3.11	Q (T*ln*1)	−3.112 ± 0.003
REINDEER (292.6 m)	−1.28	C (T*ln*2)	−1.456 ± 0.001
REINDEER (414.5 m)	1.25	C (T*ln*2)	1.215 ± 0.001
REINDEER (506 m)	3.49	FO (T*ln*1)	3.472 ± 0.003
REINDEER (597.4 m)	5.97	C (T*ln*2)	5.95 ± 0.01
MOKKA (15.2 m)	−15.371	Q (T*ln*2)	−15.50 ± 0.01
MOKKA (30.5 m)	−15.016	C (T*ln*3)	−15.117 ± 0.002
MOKKA (45.7 m)	−14.629	C (T*ln*1)	−14.717 ± 0.002
MOKKA (61 m)	−14.304	C (T*ln*2)	−14.387 ± 0.001
MOKKA (76.2 m)	−14.083	C (T*ln*2)	−14.126 ± 0.001
MOKKA (91.4 m)	−13.808	Q (T*ln*1)	−13.970 ± 0.001
MOKKA (106.7 m)	−13.265	C (T*ln*2)	−13.2982 ± 0.0001
MOKKA (152.4 m)	−11.277	C (T*ln*1)	−11.36 ± 0.01
MOKKA (198.1 m)	−9.32	Q (T*ln*1)	−9.85 ± 0.01
MOKKA (320 m)	−6.906	C (T*ln*3)	−7.50 ± 0.01
MOKKA (441.9 m)	−2.361	Q (T*ln*1)	−2.404 ± 0.001
P-RIVER (15.24 m)	−9.369	C (T*ln*3)	−9.58 ± 0.01
P-RIVER (30.48 m)	−9.167	FO (T*ln*3)	−9.2575 ± 0.0001
P-RIVER (45.72 m)	−9.052	FO (T*ln*3)	−9.43 ± 0.01
P-RIVER (60.96 m)	−8.957	FO (T*ln*3)	−9.2349 ± 0.0001
P-RIVER (91.44 m)	−8.771	FO (T*ln*3)	−9.51 ± 0.01
P-RIVER (152.4 m)	−8.124	C (T*ln*3)	−8.7031 ± 0.0001
P-RIVER (304.81 m)	−5.462	Q (T*ln*2)	−8.5378 ± 0.0001
P-RIVER (335.28 m)	−4.935	Q (T*ln*2)	−7.6325 ± 0.0001
P-RIVER (396.24 m)	−4.039	FO (T*ln*3)	−4.241 ± 0.004
P-RIVER (579.12 m)	−0.778	FO (T*ln*3)	−1.436 ± 0.001
P-RIVER (609.6 m)	−0.195	Q (T*ln*3)	−1.797 ± 0.002
P-RIVER (640.08 m)	0.761	Q (T*ln*1)	0.520 ± 0.001
P-RIVER (670.56 m)	1.664	Q (T*ln*2)	−0.018 68 ± 0.000 02
P-RIVER (701.04 m)	2.885	C (T*ln*3)	2.8578 ± 0.0003

Therefore, it is concluded that the processes of thermal recovery exhibited by most of the borehole and synthetic temperature data sets are better described by polynomial models. It was found that the larger the number of measurements, the higher the order of the polynomial that will describe this physical phenomenon. In fact, these observations are in agreement with some of the results shown in early works, which mention that the analysis of the thermal recovery process of drilled boreholes and consequently the most reliable estimation of SFT are achieved by means of the use of polynomial regression (quadratic) that must be applied in some analytical methods (e.g. Andaverde *et al* 2005 and Espinoza-Ojeda *et al* 2011).

Finally, an important observation was given in the numerical simulation of the fix model GRM (T*ln*) for the estimation of SFT. It was found that the application of %Dev $\leqslant$ 0.01 (0.01; 0.001; …), as a convergence criterion in the numerical simulation of the fix models, was very suitable and satisfactory for the cases of boreholes with temperatures higher than 100 °C (e.g. the synthetic data set CLAH). However, in the case of medium or low BHT (BHT $\leqslant$ 100 °C; e.g. the synthetic data sets CJON and SHBE), the value was not enough; therefore, it suggests that we define this parameter with a low value due to the orders of magnitude from the borehole temperatures (e.g. %Dev $\leqslant$ 0.001).

4.6. Accuracy analysis between the estimated SFTs

In this last section, an analysis of the synthetic temperature data was conducted where the SFT obtained by the log-transformation (T*ln*) method was compared with the TFT reported in the synthetic data. So, with this purpose, the synthetic data CJON, SHBE and CLAH were used; the obtained results with the new method were then compared with the estimated SFT by the analytical methods using their approximate solutions with OLS and QR models. In the accuracy evaluation, the

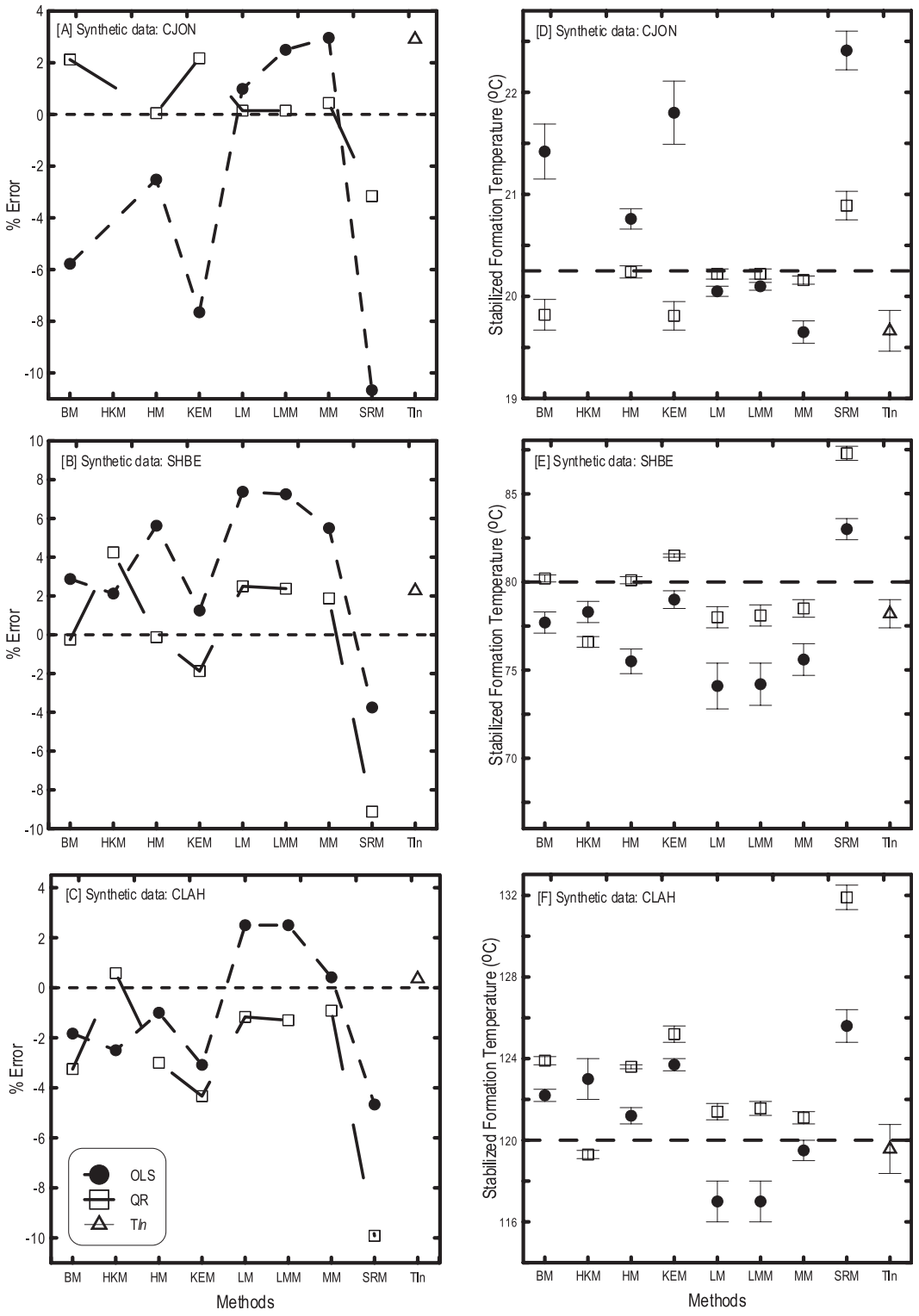

Figure 15. Results of the error percentage (%Error) between the estimated SFT (predicted with the log-transformation (T*ln*) method) and the approximate solutions of other analytical methods (using the OLS and QR models), and the TFT reported for synthetic data sets ((A): CJON; (B): SHBE; and (C): CLAH). Results of the accuracy evaluation between the SFT from the T*ln* method and the analytical methods (approximate solutions: OLS and QR), using as reference data the TFT (dashed line): (D) CJON; (E) SHBE; and (F) CLAH. The SFT uncertainties are indicated as error bars.

following statistical tests were applied: (i) the error percentage (%Error) between the estimated SFT and the TFT; and (ii) the statistical tests *F*- and Student's *t*- for significance analysis between the calculated SFT and TFT. The accuracy analysis results are shown in figure 15. The comparison between the estimated SFT and TFT through the error percentage (%Error) is shown in figures 15(A)–(C), while the results of the *F*- and Student's *t*-tests are displayed in figures 15(D)–(F). In both figures, the new method results are represented by an empty triangle symbol, while the uncertainties are shown with error

Table 13. SFT (°C) calculated by the T*ln* method, and the approximate solutions of eight analytical methods (BM, HKM, HM, KEM, LM, LMM, MM and SRM), using BHT and shut-in time data logged in geothermal boreholes.

		Methods (regression model)								
Data sets		BM	HKM	HM	KEM	LM	LMM	MM	SRM	T*ln*
CH-A$_4$	OLS	159 ± 7	153 ± 6	157 ± 8	163 ± 7	153 ± 9	154 ± 9	144 ± 11	176 ± 8	181 ± 2
(BHT$_n$ = 169 °C)	QR	175.0 ± 3.1	159 ± 5	172.9 ± 3.4	178.6 ± 2.9	170.0 ± 4.1	170.1 ± 4.0	163 ± 6	207 ± 5	
CH-A$_9$	OLS	132.1 ± 4.2	128.9 ± 3.7	130.7 ± 4.5	133.9 ± 3.8	129 ± 5	129 ± 5	125 ± 6	141.2 ± 4.4	148 ± 1
(BHT$_n$ = 138 °C)	QR	140.3 ± 2.8	131.8 ± 3.4	139.0 ± 3.2	142.5 ± 2.4	137.2 ± 3.6	137.4 ± 3.5	133.7 ± 4.3	157.8 ± 2.3	
CH-A$_{11}$	OLS	137 ± 6	134 ± 5	136 ± 6	139 ± 5	134 ± 6	134 ± 6	129 ± 7	146 ± 6	159 ± 2
(BHT$_n$ = 145 °C)	QR	148.4 ± 2.9	138.3 ± 3.6	146.7 ± 3.4	151.2 ± 2.1	144.6 ± 3.9	144.6 ± 3.9	140 ± 5	170.4 ± 1.6	
MXCO$_1$	OLS	256 ± 5	256.9 ± 2.0	253 ± 6	262 ± 5	251 ± 6	251 ± 6	246 ± 6	283 ± 7	263 ± 3
(BHT$_n$ = 247.7 °C)	QR	281 ± 5	263.1 ± 2.4	278 ± 5	290 ± 5	276 ± 5	276 ± 5	270 ± 5	340 ± 8	
MXCO$_2$	OLS	254 ± 5	252.9 ± 2.0	251 ± 6	260 ± 5	249 ± 6	249 ± 6	244 ± 6	301 ± 5	262 ± 3
(BHT$_n$ = 247.1 °C)	QR	279.4 ± 3.5	259.3 ± 1.7	277.0 ± 3.5	288 ± 3	274.3 ± 3.7	274.5 ± 3.6	269 ± 4	352 ± 16	
ITAL	OLS	130.6 ± 0.6	128.82 ± 0.12	127.8 ± 0.6	134.2 ± 0.6	124.8 ± 0.6	124.6 ± 0.6	120.1 ± 0.7	142.2 ± 0.6	120 ± 1
(BHT$_n$ = 118.7 °C)	QR	133.4 ± 1.9	128.08 ± 0.35	132.2 ± 1.6	135.8 ± 2.5	130.0 ± 1.3	133.31 ± 0.44	123.0 ± 0.9	161.9 ± 1.1	
PHIL	OLS	206.7 ± 4.2	150.4 ± 3.9	182.3 ± 3.1	197 ± 5	149.3 ± 3.9	187.9 ± 3.1		179 ± 6	158 ± 2
(BHT$_n$ = 146 °C)	QR	233 ± 23	178.3 ± 3.0	211 ± 15	251 ± 18	176.9 ± 2.8	189 ± 14		249 ± 10	
JAPN	OLS	172 ± 4	169.2 ± 1.5	167 ± 4	178 ± 3	162 ± 5	162 ± 5	157 ± 7	209.9 ± 0.9	176 ± 2
(BHT$_n$ = 170.9 °C)	QR	187 ± 2	171.8 ± 1.6	184.7 ± 2.5	192 ± 1	180.1 ± 3.4	180.3 ± 3.3	162 ± 6	215	
CB-1 (994 m,	OLS	53.35 ± 0.38	53.75 ± 0.25	53.20 ± 0.39	53.76 ± 0.39	53.05 ± 0.39	53.07 ± 0.39	52.71 ± 0.41	54.9 ± 0.6	58 ± 1
BHT$_n$ = 52.3 °C)	QR	55 ± 1	53.83 ± 1.13	55 ± 1	55.42 ± 1.37	54.6 ± 0.8	54.6 ± 0.8	54.3 ± 0.6	58.18 ± 2.88	
CB-1 (1494 m,	OLS	72.3 ± 0.6	72.27 ± 0.23	71.3 ± 0.7	73.7 ± 0.5	70.1 ± 0.8	70.1 ± 0.8	67.96 ± 1.06	77.3 ± 0.8	79 ± 1
BHT$_n$ = 65.8 °C)	QR	75.58	71.17	75.01	76.83	74.06	74.06	72.32	84.13	
CB-1 (1987 m,	OLS	94.16 ± 1.56	94.08 ± 0.29	93.15 ± 1.76	95.4 ± 1.5	92.07 ± 1.93	92.13 ± 1.91	89.55 ± 2.35	98.04 ± 2.17	98 ± 1
BHT$_n$ = 90 °C)	QR	98.81	94.78	97.94	100.55	96.79	96.81	94.6	108.4	
CB-1 (2583 m,	OLS	107.1 ± 2.9	109.7 ± 1.7	106.2 ± 2.9	109.6 ± 3.0	105.3 ± 2.9	105.4 ± 2.9	103.3 ± 2.9	116.3 ± 4.1	108.48 ± 0.01
BHT$_n$ = 102.7 °C)	QR	120 ± 6	116 ± 5	118 ± 6	124 ± 7.0	117 ± 5	117 ± 5	114 ± 5	146 ± 13	
R #9-1	OLS	212.3 ± 4.1	181.2 ± 1.4	205.9 ± 3.1	216.6 ± 4.5	198.3 ± 2.1	198.3 ± 2.1	185.5 ± 0.6	205.1 ± 0.8	173 ± 2
(BHT$_n$ = 170 °C)	QR	156 ± 10	174.3 ± 1.8	168 ± 8	149 ± 12	178 ± 5	178 ± 5	185.9 ± 2.4	258.4	
SGIL	OLS	100.5 ± 0.1	109.7 ± 1.8	99.3 ± 0.2	102.1 ± 0.2	97.0 ± 0.4	97.32 ± 0.37	97.5 ± 0.2	102.9 ± 0.3	102 ± 1
(BHT$_n$ = 96.13 °C)	QR	100.0 ± 0.3	81.9 ± 2.5	99 ± 1	101.1 ± 0.5	99.1 ± 0.2	99.22 ± 0.18	98.3 ± 0.2	104 ± 1	
ROUX	OLS	200 ± 9	198.9 ± 10.3	185 ± 5	186 ± 5	172.18 ± 2.16	172.17 ± 2.15		195 ± 6	180 ± 2
(BHT$_n$ = 155.56 °C)	QR	75.32	64.26	132.91	128.16	155.3	155.32		111.21	

Table 14. SFT (°C) calculated by the T*ln* method, and the approximate solutions from analytical methods (BM, HKM, HM, KEM, LM, LMM, MM and SRM), using BHT and shut-in time data from the geothermal boreholes KELLEY and GT-2, and the synthetic data sets CJON, SHBE and CLAH.

		Methods (regression model)								
Data sets		BM	HKM	HM	KEM	LM	LMM	MM	SRM	T*ln*
KELLEY	OLS	110.57 ± 1.76	104.7 ± 0.8	107.35 ± 1.94	108.10 ± 1.92	103.62 ± 2.04	103.62 ± 2.04	97.18 ± 2.28	118.11 ± 2.69	112 ± 1
($BHT_n = 94.44$ °C)	QR	124.75	108.61	121.17	122.25	115.89	115.91	107.81	148.53	
GT-2	OLS	126.75 ± 0.11	124.77 ± 0.11	126.2 ± 0.1	127.39 ± 0.14	125.539 ± 0.042	125.554 ± 0.043	123.91 ± 0.10	129.72 ± 0.17	124 ± 1
(1595 m, $BHT_n = 123.817$ °C)	QR	124.73 ± 0.15	123.8 ± 0.1	125.08 ± 0.10	124.48 ± 0.18	125.2 ± 0.1	125.18 ± 0.08	124.9 ± 0.1	124.79 ± 0.27	
CJON	OLS	21.42 ± 0.27		20.76 ± 0.10	21.80 ± 0.31	20.05 ± 0.05	20.099 ± 0.038	19.65 ± 0.11	22.41 ± 0.19	19.7 ± 0.2
(TFT = 20.25 °C)	QR	19.82 ± 0.15		20.24 ± 0.06	19.81 ± 0.14	20.22 ± 0.05	20.22 ± 0.05	20.16 ± 0.04	20.89 ± 0.14	
SHBE	OLS	77.7 ± 0.6	78.3 ± 0.6	75.5 ± 0.7	79.0 ± 0.5	74.1 ± 1.3	74.2 ± 1.2	75.6 ± 0.9	83.0 ± 0.6	78 ± 1
(TFT = 80 °C)	QR	80.2 ± 0.2	76.6 ± 0.3	80.1 ± 0.2	81.5 ± 0.1	78.0 ± 0.6	78.1 ± 0.6	78.5 ± 0.5	87.3 ± 0.4	
CLAH	OLS	122.2 ± 0.3	123 ± 1	121.2 ± 0.4	123.7 ± 0.3	117 ± 1	117 ± 1	119.5 ± 0.5	125.6 ± 0.8	120 ± 1
(TFT = 120 °C)	QR	123.9 ± 0.2	119.3 ± 0.2	123.6 ± 0.1	125.2 ± 0.4	121.4 ± 0.4	121.56 ± 0.34	121.1 ± 0.3	131.9 ± 0.6	

Table 15. SFT (°C) calculated by the T*ln* method, and the approximate solutions from analytical methods (BM, HKM, HM, KEM, LM, LMM, MM and SRM), using BHT and shut-in time data logged from petroleum boreholes.

		Methods (regression model)								
Data sets		BM	HKM	HM	KEM	LM	LMM	MM	SRM	T*ln*
COST (1420 m,	OLS	60.3 ± 1.9	59.5 ± 2.4	60.0 ± 1.7	60.9 ± 2.2	59.5 ± 1.4	59.52 ± 1.45	58.7 ± 1.0		61 ± 1
$BHT_n = 56.11$ °C)	QR	53.2 ± 1.2	54.0 ± 2.2	54 ± 1	51.9 ± 1.7	54.8 ± 0.7	54.8 ± 0.7	56.3 ± 0.7		
COST (3710 m,	OLS	156.8 ± 2.0	156.6 ± 3.2	155.2 ± 2.0	159.4 ± 2.1	153.3 ± 2.3	153.4 ± 2.2	149.4 ± 3.0	170.0 ± 2.8	166 ± 2
$BHT_n = 150$ °C)	QR	158 ± 5	149 ± 5	158.0 ± 4.4	159 ± 6	157.3 ± 3.9	157.3 ± 3.9	155.6 ± 3.2	170 ± 12	
COST (4475 m,	OLS	186.36 ± 2.61	180.58 ± 1.84	184.8 ± 2.3	189.38 ± 3.13	183.13 ± 2.07	183.3 ± 2.1	179.9 ± 1.6	196.4 ± 4.2	188 ± 2
$BHT_n = 174.44$ °C)	QR	179.29 ± 26.05	177 ± 11	180.0 ± 22.4	178 ± 35	180.3 ± 18.7	180 ± 19	180 ± 13	177 ± 63	
USAM	OLS	145.7 ± 0.3	145.8 ± 0.3	146.0 ± 0.4	145.9 ± 0.3	144.8 ± 0.5	144.8 ± 0.5	146.0 ± 0.4	147.5 ± 0.4	149.2 ± 0.2
($BHT_n = 147.27$ °C)	QR	146.7 ± 0.3	146.0 ± 0.3	147.1 ± 0.3	147.0 ± 0.3	145.5 ± 0.4	145.61 ± 0.39	147.1 ± 0.3	148.0 ± 0.3	
MALOOB—309D	OLS	113.8 ± 4.3		113.8 ± 4.3	113.8 ± 4.3	113.8 ± 4.3	113.8 ± 4.3	113.7 ± 4.2	120 ± 8	127 ± 1
($BHT_n = 118$ °C)	QR	132 ± 9		132 ± 9	132 ± 9	132 ± 9	132 ± 9	132 ± 9	152.2 ± 23.6	
MALOOB—456	OLS	119 ± 5		119 ± 5	119 ± 5	119 ± 5	119 ± 5	119 ± 5	128 ± 6	136 ± 1
($BHT_n = 127$ °C)	QR	142 ± 5		142 ± 5	142 ± 5	142 ± 5	142 ± 5	142 ± 5	178 ± 13	
Franciacorta (3328 m,	OLS	93.4 ± 0.7	94.78 ± 0.18	93.2 ± 0.7	94.2 ± 0.6	92.9 ± 0.7	93.0 ± 0.7	92.4 ± 0.8	96.6 ± 0.8	101 ± 1
$BHT_n = 92$ °C)	QR	95.6 ± 0.5	94.21 ± 0.34	95.4 ± 0.5	96.47 ± 0.44	95.2 ± 0.5	95.3 ± 0.5	94.7 ± 0.6	101.1 ± 0.6	
BECU	OLS	87.21 ± 1.34	76 ± 1	81.0 ± 1.5	87.6 ± 1.6	76.7 ± 1.4	76.7 ± 1.4		84.5 ± 2.0	86 ± 1
($BHT_n = 72$ °C)	QR	103 ± 6	80 ± 1	94.2 ± 2.4	108 ± 6	86 ± 1	86 ± 1		108.5 ± 3.7	

Table 16. SFT (°C) calculated by the T*ln* method, and the approximate solutions from analytical methods (BM, HM, KEM, LM, LMM, MM and SRM), using BHT and shut-in time data logged from permafrost borehole REINDEER.

		Methods (regression model)							
Data sets		BM	HM	KEM	LM	LMM	MM	SRM	T*ln*
REINDEER (18.3 m, $BHT_n = -7.69$ °C)	OLS	-7.50 ± 0.17	-7.30 ± 0.16	-7.33 ± 0.16	-7.04 ± 0.16	-7.04 ± 0.16	-6.53 ± 0.20	-8.96 ± 0.25	-9.12 ± 0.01
	QR	-7.37 ± 0.39	-7.36 ± 0.37	-7.37 ± 0.37	-7.32 ± 0.34	-7.33 ± 0.35	-7.22 ± 0.31	-8.1 ± 0.8	
REINDEER (48.8 m, $BHT_n = -5.58$ °C)	OLS	-6.2 ± 0.1	-6.1 ± 0.1	-6.1 ± 0.1	-5.86 ± 0.03	-5.87 ± 0.03	-5.5 ± 0.1	-7.4 ± 0.2	-5.67 ± 0.01
	QR	-5.69 ± 0.03	-5.72 ± 0.02	-5.72 ± 0.02	-5.74 ± 0.02	-5.74 ± 0.02	-5.74 ± 0.01	-5.5 ± 0.1	
REINDEER (79.2 m, $BHT_n = -5.14$ °C)	OLS	-5.7 ± 0.1	-5.6 ± 0.1	-5.6 ± 0.1	-5.4 ± 0.1	-5.36 ± 0.10	-4.9 ± 0.2	-6.8 ± 0.2	-5.25 ± 0.01
	QR	-5.6 ± 0.2	-5.6 ± 0.1	-5.6 ± 0.1	-5.6 ± 0.1	-5.63 ± 0.12	-5.5 ± 0.1	-6.0 ± 0.4	
REINDEER (140.2 m, $BHT_n = -4.3$ °C)	OLS	-4.4 ± 0.2	-4.2 ± 0.2	-4.2 ± 0.2	-4.0 ± 0.3	-4.03 ± 0.26	-3.6 ± 0.3	-5.3 ± 0.3	-5.70 ± 0.01
	QR	-5.2 ± 0.1	-5.1 ± 0.1	-5.1 ± 0.1	-5.0 ± 0.1	-5.0 ± 0.1	-4.70 ± 0.04	-6.9 ± 0.4	
REINDEER (201.2 m, $BHT_n = -3.11$ °C)	OLS	-3.33 ± 0.03	-3.24 ± 0.04	-3.26 ± 0.04	-3.1 ± 0.1	-3.12 ± 0.07	-2.8 ± 0.1	-3.9 ± 0.1	-3.112 ± 0.003
	QR	-3.39 ± 0.04	-3.39 ± 0.04	-3.39 ± 0.04	-3.36 ± 0.02	-3.36 ± 0.03	-3.278 ± 0.004	-3.8 ± 0.1	
REINDEER (292.6 m, $BHT_n = -1.28$ °C)	OLS	-1.2 ± 0.1	-1.1 ± 0.1	-1.2 ± 0.1	-1.1 ± 0.1	-1.1 ± 0.1	-0.97 ± 0.11	-1.5 ± 0.1	-1.456 ± 0.001
	QR	-1.5 ± 0.1	-1.5 ± 0.1	-1.5 ± 0.1	-1.4 ± 0.1	-1.42 ± 0.06	-1.3 ± 0.1	-2.2 ± 0.1	
REINDEER (414.5 m, $BHT_n = 1.25$ °C)	OLS	1.07 ± 0.01	1.129 ± 0.003	1.118 ± 0.002	1.22 ± 0.02	1.21 ± 0.02	1.4 ± 0.1	0.64 ± 0.04	1.215 ± 0.001
	QR	1.124 ± 0.003	1.119 ± 0.003	1.118 ± 0.002	1.129 ± 0.003	1.126 ± 0.003	1.17 ± 0.01	0.95 ± 0.02	
REINDEER (506 m, $BHT_n = 3.49$ °C)	OLS	3.32 ± 0.02	3.378 ± 0.002	3.368 ± 0.003	3.46 ± 0.02	3.46 ± 0.02	3.6 ± 0.1	2.92 ± 0.04	3.472 ± 0.003
	QR	3.382 ± 0.004	3.376 ± 0.003	3.375 ± 0.003	3.385 ± 0.004	3.382 ± 0.004	3.42 ± 0.01	3.22 ± 0.02	
REINDEER (597.4 m, $BHT_n = 5.97$ °C)	OLS	5.81 ± 0.01	5.867 ± 0.003	5.858 ± 0.004	5.94 ± 0.02	5.94 ± 0.02	6.1 ± 0.1	5.44 ± 0.04	5.95 ± 0.01
	QR	5.87 ± 0.01	5.868 ± 0.005	5.867 ± 0.005	6 ± 0	5.873 ± 0.004	5.91 ± 0.01	5.74 ± 0.02	

Table 17. SFT (°C) calculated by the T*ln* method, and the approximate solutions from analytical methods (BM, HM, KEM, LM, LMM, MM and SRM), using BHT and shut-in time data logged from permafrost borehole MOKKA.

		Methods (regression model)							
Data sets		BM	HM	KEM	LM	LMM	MM	SRM	T*ln*
MOKKA (18.3 m, $BHT_n = -15.371$ °C)	OLS	-15.6 ± 0.1	-15.18 ± 0.13	-15.21 ± 0.12	-14.94 ± 0.18	-14.94 ± 0.18	-15.50 ± 0.16	-15.61 ± 0.11	-15.50 ± 0.01
	QR	-15.58 ± 0.19	-15.58 ± 0.18	-15.58 ± 0.18	-15.54 ± 0.17	-15.55 ± 0.17	-15.5 ± 0.5	-16.25 ± 0.33	
MOKKA (30.5 m, $BHT_n = -15.016$ °C)	OLS	-15.04 ± 0.14	-14.53 ± 0.18	-14.57 ± 0.17	-14.21 ± 0.26	-14.21 ± 0.26	-14.66 ± 0.21	-14.86 ± 0.18	-15.117 ± 0.002
	QR	-14.90 ± 0.21	-14.87 ± 0.19	-14.90 ± 0.19	-14.78 ± 0.20	-14.79 ± 0.20	-15.13 ± 0.19	-15.59 ± 0.25	
MOKKA (45.7 m, $BHT_n = -14.629$ °C)	OLS	-14.6 ± 0.1	-14.21 ± 0.17	-14.24 ± 0.16	-13.96 ± 0.24	-13.96 ± 0.24	-14.42 ± 0.14	-14.47 ± 0.17	-14.717 ± 0.002
	QR	-14.66 ± 0.10	-14.6 ± 0.1	-14.6 ± 0.1	-14.53 ± 0.12	-14.54 ± 0.12	-14.790 ± 0.044	-15.3 ± 0.1	
MOKKA (61 m, $BHT_n = -14.304$ °C)	OLS	-14.5 ± 0.1	-14.04 ± 0.21	-14.07 ± 0.20	-13.77 ± 0.30	-13.75 ± 0.30	-14.31 ± 0.16	-14.29 ± 0.22	-14.387 ± 0.001
	QR	-14.58 ± 0.11	-14.54 ± 0.11	-14.56 ± 0.11	-14.44 ± 0.13	-14.44 ± 0.13	-14.64 ± 0.11	-15.25 ± 0.16	
MOKKA (76.2 m, $BHT_n = -14.083$ °C)	OLS	-14.2 ± 0.1	-13.79 ± 0.17	-13.82 ± 0.17	-13.53 ± 0.25	-13.53 ± 0.25	-14.01 ± 0.15	-14.05 ± 0.18	-14.126 ± 0.001
	QR	-14.25 ± 0.12	-14.22 ± 0.12	-14.23 ± 0.12	-14.12 ± 0.13	-14.13 ± 0.13	-14.35 ± 0.11	-14.88 ± 0.18	
MOKKA (91.4 m, $BHT_n = -13.808$ °C)	OLS	-14.005 ± 0.022	-13.62 ± 0.16	-13.65 ± 0.15	-13.38 ± 0.25	-13.38 ± 0.25	-13.812 ± 0.028	-13.89 ± 0.17	-13.970 ± 0.001
	QR	-13.983 ± 0.029	-13.976 ± 0.024	-13.985 ± 0.027	-13.90 ± 0.01	-13.90 ± 0.01	-13.900 ± 0.014	-14.60 ± 0.13	
MOKKA (106.7 m, $BHT_n = -13.265$ °C)	OLS	-13.4 ± 0.1	-12.99 ± 0.18	-13.02 ± 0.17	-12.72 ± 0.26	-12.72 ± 0.26	-13.23 ± 0.13	-13.26 ± 0.19	-13.2982 ± 0.0001
	QR	-13.5 ± 0.1	-13.4 ± 0.1	-13.5 ± 0.1	-13.35 ± 0.10	-13.35 ± 0.10	-13.5 ± 0.1	-14.14 ± 0.15	
MOKKA (152.4 m, $BHT_n = -11.277$ °C)	OLS	-11.2 ± 0.1	-10.92 ± 0.16	-10.94 ± 0.15	-10.73 ± 0.22	-10.73 ± 0.22	-11.07 ± 0.13	-11.11 ± 0.17	-11.36 ± 0.01
	QR	-11.25 ± 0.14	-11.23 ± 0.13	-11.23 ± 0.13	-11.15 ± 0.13	-11.15 ± 0.13	-11.40 ± 0.21	-11.78 ± 0.16	
MOKKA (198.1 m, $BHT_n = -7.895$ °C)	OLS	-9.44 ± 0.26	-9.22 ± 0.25	-9.24 ± 0.25	-9.08 ± 0.25	-9.08 ± 0.25	-9.34 ± 0.31	-9.36 ± 0.27	-9.85 ± 0.01
	QR	-9.34 ± 0.40	-9.38 ± 0.37	-9.38 ± 0.37	-9.37 ± 0.34	-9.37 ± 0.34	-9.1 ± 0.5	-10 ± 1	
MOKKA (320 m, $BHT_n = -6.906$ °C)	OLS	-6.17 ± 0.39	-6.03 ± 0.37	-6.04 ± 0.37	-5.97 ± 0.36	-5.97 ± 0.36	-6.71 ± 0.18	-6.05 ± 0.39	-7.50 ± 0.01
	QR	-7.3 ± 0.1	-7.06 ± 0.11	-7.09 ± 0.11	-6.88 ± 0.15	-6.89 ± 0.15	-7.20 ± 0.11	-8.1 ± 0.1	
MOKKA (441.9 m, $BHT_n = -2.361$ °C)	OLS	-1.73 ± 0.28	-1.77 ± 0.22	-1.77 ± 0.23	-1.82 ± 0.19	-1.82 ± 0.19	-2.19 ± 0.11	-1.70 ± 0.23	-2.404 ± 0.001
	QR	-2.5 ± 0.1	-2.4 ± 0.1	-2.4 ± 0.1	-2.3 ± 0.1	-2.3 ± 0.1	-2.4 ± 0.1	-2.85 ± 0.11	

Table 18. SFT (°C) calculated by the T*ln* method, and the approximate solutions from analytical methods (BM, HM, KEM, LM, LMM, MM and SRM), using BHT and shut-in time data logged from permafrost borehole P-RIVER.

Data sets		Methods (regression model)							
		BM	HM	KEM	LM	LMM	MM	SRM	T*ln*
P-RIVER	OLS	-11 ± 1	-9.43 ± 0.27	-9.59 ± 0.25	-8 ± 1	-8.1 ± 0.1	-9 ± 1	-10.05 ± 0.36	-9.58 ± 0.01
(15.24 m, $BHT_n = -9.369$ °C)	QR	-10 ± 1	-9.82 ± 0.37	-9.86 ± 0.39	-9.27 ± 0.31	-9.27 ± 0.31	-10 ± 1	-11 ± 1	
P-RIVER	OLS	-10.41 ± 0.38	-9.16 ± 0.34	-9.33 ± 0.32	-8 ± 1	-7.7 ± 0.1	-8.75 ± 0.27	-10 ± 1	-9.2575 ± 0.0001
(30.48 m, $BHT_n = -9.167$ °C)	QR	-9.54 ± 0.43	-9.89 ± 0.38	-9.94 ± 0.41	-9.27 ± 0.21	-9.27 ± 0.21	-9.33 ± 0.16	-11 ± 1	
P-RIVER	OLS	-10.29 ± 0.41	-8.98 ± 0.42	-9.16 ± 0.40	-8 ± 1	-7.5 ± 0.1	-8.62 ± 0.24	-10 ± 1	-9.43 ± 0.01
(45.72 m, $BHT_n = -9.052$ °C)	QR	-10 ± 1	-10 ± 1	-10 ± 1	-9.21 ± 0.23	-9.21 ± 0.23	-9.2 ± 0.1	-11 ± 1	
P-RIVER	OLS	-10.16 ± 0.40	-8.99 ± 0.26	-9.15 ± 0.24	-8 ± 1	-7.6 ± 0.1	-8.51 ± 0.23	-9.59 ± 0.38	-9.2349 ± 0.0001
(60.96 m, $BHT_n = -8.957$ °C)	QR	-9.12 ± 0.36	-9.49 ± 0.32	-9.53 ± 0.34	-8.96 ± 0.19	-8.96 ± 0.19	-9.0 ± 0.1	-11 ± 1	
P-RIVER	OLS	-9.89 ± 0.41	-9 ± 1	-9 ± 1	-7 ± 1	-7.1 ± 0.1	-8.30 ± 0.23	-9 ± 1	-9.51 ± 0.01
(91.44 m, $BHT_n = -8.771$ °C)	QR	-9 ± 1	-10 ± 1	-10 ± 1	-8.91 ± 0.23	-8.91 ± 0.23	-8.8 ± 0.1	-11 ± 1	
P-RIVER	OLS	-8.52 ± 0.37	-7 ± 1	-7 ± 1	-6 ± 1	-5.6 ± 0.1	-7.53 ± 0.33	-8 ± 1	-8.7031 ± 0.0001
(152.4 m, $BHT_n = -8.124$ °C)	QR	-9 ± 1	-8.93 ± 0.29	-9.05 ± 0.33	-7.74 ± 0.37	-7.74 ± 0.37	-8.274 ± 0.021	-11 ± 1	
P-RIVER	OLS	-5 ± 1	-3.8 ± 1.2	-3.9 ± 1.2	-2.5 ± 1.3	-2.5 ± 1.3		-4.0 ± 1.3	-8.5378 ± 0.0001
(304.81 m, $BHT_n = -5.462$ °C)	QR	-5.8 ± 0.6	-5.4 ± 0.9	-5.5 ± 0.9	-4.7 ± 1.3	-4.7 ± 1.3		-6 ± 1	
P-RIVER	OLS	-4.5 ± 0.7	-3.5 ± 1.1	-3.6 ± 1.0	-2.3 ± 1.2	-2.3 ± 1.2		-3.7 ± 1.2	-7.6325 ± 0.0001
(335.28 m, $BHT_n = -4.935$ °C)	QR	-5.2 ± 0.6	-4.9 ± 0.9	-4.9 ± 0.8	-4.2 ± 1.2	-4.2 ± 1.2		-5.8 ± 0.9	
P-RIVER	OLS	-3.36 ± 0.35	-2.64 ± 0.40	-2.73 ± 0.39	-1.94 ± 0.43	-1.94 ± 0.43	-3 ± 1	-3 ± 1	-4.241 ± 0.004
(396.24 m, $BHT_n = -4.039$ °C)	QR	-4 ± 1	-3 ± 1	-4 ± 1	-3 ± 1	-2.7 ± 0.1	-4.03 ± 0.28	-4 ± 1	
P-RIVER	OLS	-1.28 ± 0.39	-1.06 ± 0.20	-1.10 ± 0.22	-0.7 ± 0.1	-0.7 ± 0.1	-0.6 ± 0.1	-1.30 ± 0.19	-1.436 ± 0.001
(579.12 m, $BHT_n = -0.778$ °C)	QR	-0.29 ± 0.38	-0.52 ± 0.13	-0.50 ± 0.14	-0.6 ± 0.1	-0.6 ± 0.1	-1 ± 1	-0.57 ± 0.14	
P-RIVER	OLS	-0.52 ± 0.16	0.00 ± 0.24	-0.06 ± 0.23	0.54 ± 0.30	0.54 ± 0.30	-0.1 ± 0.1	-0.19 ± 0.30	-1.797 ± 0.002
(609.6 m, $BHT_n = -0.195$ °C)	QR	-0.61 ± 0.27	-0.64 ± 0.16	-0.67 ± 0.18	-0.3 ± 0.1	-0.3 ± 0.1	-0.262 ± 0.032	-1.24 ± 0.31	
P-RIVER	OLS	0.20 ± 0.17	1.07 ± 0.24	0.96 ± 0.22	2.05 ± 0.41	2.05 ± 0.41	1.22 ± 0.23	0.67 ± 0.33	0.520 ± 0.001
(640.08 m, $BHT_n = 0.761$ °C)	QR	0.53 ± 0.23	0.45 ± 0.18	0.40 ± 0.20	0.97 ± 0.17	0.97 ± 0.17	0.7 ± 0.1	-0.47 ± 0.34	
P-RIVER	OLS	0.8 ± 0.9	1.59 ± 0.23	1.46 ± 0.24	3.0 ± 0.7	3.0 ± 0.7		1.26 ± 0.28	$-0.018\,68 \pm 0.000\,02$
(670.56 m, $BHT_n = 1.664$ °C)	QR	1.7 ± 0.5	1.56 ± 0.37	1.55 ± 0.38	1.76 ± 0.40	1.76 ± 0.40		1 ± 1	
P-RIVER	OLS	2.04 ± 0.36	2.94 ± 0.16	2.81 ± 0.15	4.06 ± 0.41	4.06 ± 0.41	4.06 ± 0.41	3.25 ± 0.26	2.8578 ± 0.0003
(701.04 m, $BHT_n = 2.885$ °C)	QR	2.87 ± 0.27	2.66 ± 0.20	2.64 ± 0.21	3.06 ± 0.19	3.06 ± 0.19	3.06 ± 0.19	2.818 ± 0.037	

Table 19. SFT (°C) calculated by the T*ln* method, and the average SFT by the use of the OLS and QR models for the approximate solutions of eight analytical methods (BM, HKM, HM, KEM, LM, LMM, MM and SRM), using BHT and shut-in time data logged in geothermal boreholes, and the synthetic data sets CJON, SHBE and CLAH. Outliners indicated by 'a' and 'b', see footnote.

	Analytical methods		Empirical method
Data sets	OLS	QR	T*ln*
CH-A$_4$ (BHT$_n$ = 169 °C)	157 ± 9	170 ± 7[a]	181 ± 2
CH-A$_9$ (BHT$_n$ = 138 °C)	131 ± 5	137.4 ± 3.7[a]	148 ± 1
CH-A$_{11}$ (BHT$_n$ = 145 °C)	136 ± 5	145 ± 5[a]	159 ± 2
MXCO$_1$ (BHT$_n$ = 247.7 °C)	254 ± 5[a]	276 ± 8[a]	263 ± 3
MXCO$_2$ (BHT$_n$ = 247.1 °C)	251 ± 5[a]	275 ± 9[a]	262 ± 3
ITAL (BHT$_n$ = 118.7 °C)	129 ± 7	130.8 ± 4.3[a]	120 ± 1
PHIL (BHT$_n$ = 146 °C)	178.9 ± 21.9	212.6 ± 32.2	158 ± 2
JAPN (BHT$_n$ = 170.9 °C)	167 ± 7[a]	184.1 ± 15.6	176 ± 2
CB-1 (994 m, BHT$_n$ = 52.3 °C)	53.5 ± 0.7	55 ± 1[a]	58 ± 1
CB-1 (1494 m, BHT$_n$ = 65.8 °C)	71.9 ± 2.8	75.4 ± 4.0	79 ± 1
CB-1 (1987 m, BHT$_n$ = 90 °C)	93.57 ± 2.52	98.6 ± 4.4	98 ± 1
CB-1 (2583 m, BHT$_n$ = 102.7 °C)	107.9 ± 4.0	118.0 ± 3.2[a]	108 ± 1
R #9-1 (BHT$_n$ = 170 °C)	200.4 ± 12.3	169.9 ± 13.2[a]	173 ± 2
SGIL (BHT$_n$ = 96.13 °C)	100.8 ± 4.2	100.1 ± 1.9	102 ± 1
ROUX (BHT$_n$ = 155.56 °C)	187.0 ± 11.7	117.5 ± 36.2	180 ± 2
KELLEY (BHT$_n$ = 94.44 °C)	106.7 ± 6.1	120.6 ± 12.8	112 ± 1
GT-2 (1595 m, BHT$_n$ = 123.817 °C)	126.23 ± 1.78	125 ± 1	124 ± 1
CJON (TEFV = 20.25 °C)	20.88 ± 1.03	20.08 ± 0.21[a]	19.7 ± 0.2
SHBE (TEFV = 80 °C)	77.2 ± 3.0	80.04 ± 3.32	78 ± 1
CLAH (TEFV = 120 °C)	121.15 ± 3.12	123.50 ± 3.88	120 ± 1

[a] SFT (SRM) outlier.
[b] SFT (HKM) outlier.

Table 20. SFT (°C) calculated by the T*ln* method, and the average SFT by the use of the OLS and QR models for the approximate solutions of eight analytical methods (BM, HKM, HM, KEM, LM, LMM, MM and SRM), using BHT and shut-in time data logged in petroleum boreholes. Outliners indicated by 'a', described in footnote.

	Analytical methods		Empirical method
Data sets	OLS	QR	T*ln*
COST (1420 m, BHT$_n$ = 56.11 °C)	59.8 ± 0.7	54.14 ± 1.38	61 ± 1
COST (3710 m, BHT$_n$ = 150 °C)	157 ± 6	156.31 ± 3.39[a]	166 ± 2
COST (4475 m, BHT$_n$ = 174.44 °C)	186 ± 5	178.95 ± 1.40	188 ± 2
USAM (BHT$_n$ = 147.27 °C)	146 ± 1[a]	146.6 ± 0.9	149.2 ± 0.2
MALOOB—309D (BHT$_n$ = 118 °C)	113.8 ± 0[a]	132 ± 0[a]	127 ± 1
MALOOB—456 (BHT$_n$ = 127 °C)	119 ± 0[a]	142 ± 0[a]	136 ± 1
Franciacorta (3328 m, BHT$_n$ = 92 °C)	93.81 ± 1.36	95 ± 1[a]	101 ± 1
BECU (BHT$_n$ = 72 °C)	81 ± 5	95.1 ± 11.6	86 ± 1

[a] SFT (SRM) outlier.

bars (see figures 15(D)–(F)). As a reference the calculated SFTs by the analytical methods are included.

After analyzing the global results of these tests, it was found that only in the case of CLAH (see figures 15(C) and (F)) did the new method provide a most suitable estimation with a lower error percentage of 0.36%. The SFT estimated with the new method (SFT = 120 ± 1 °C: SI(T*ln*2)) was compared with the reported TFT (120 °C) through the *F*- and Student's *t*-tests. The obtained results from this analysis do not show such significant differences that make the null hypothesis (H$_0$) acceptable. The deviation percentages found by the GRM (T*ln*) models (figures 15(A) and (B)) are inside of the ±3% of the average deviation.

In the case of the data set CJON (TFT = 20.25 °C; SFT = 19.7 ± 0.2 °C: *C*(T*ln*1)), the new method provides predictions with the highest average error of 2.9%, when it is compared with the TFT (figure 15(A)), while with the SHBE (TFT = 80 °C; SFT = 78 ± 1 °C: FO(T*ln*2)), the comparison error with the TFT was 2.3% (figure 15(B)). Also, it can be observed that lower error percentages (between −3.1% and 2.5%) were obtained for the data set CLAH (figure 15(C)), while the highest values (between −10% and 8%) were reached

Table 21. SFT (°C) calculated by the T*ln* method, and the average SFT by the use of the OLS and QR models for the approximate solutions of seven analytical methods (BM, HM, KEM, LM, LMM, MM and SRM), using BHT and shut-in time data logged in the permafrost boreholes REINDEER, MOKKA and P-RIVER. Outliners indicated by 'a', 'b', 'c' and 'd', see footnote.

	Analytical methods		Empirical method
Data sets	OLS	QR	T*ln*
REINDEER (18.3 m, $BHT_n = -7.69$ °C)	-7.12 ± 0.34[a]	-7.3 ± 0.1[a]	-9.117 ± 0.01
REINDEER (48.8 m, $BHT_n = -5.58$ °C)	-5.93 ± 0.25[a]	-5.73 ± 0.02[a]	-5.67 ± 0.01
REINDEER (79.2 m, $BHT_n = -5.14$ °C)	-5.43 ± 0.29[a]	-5.65 ± 0.16[c]	-5.250 ± 0.01
REINDEER (140.2 m, $BHT_n = -4.3$ °C)	-4.3 ± 0.5	-5.02 ± 0.17[a]	-5.701 ± 0.01
REINDEER (201.2 m, $BHT_n = -3.11$ °C)	-3.25 ± 0.33	-3.36 ± 0.04[a]	-3.112 ± 0.003
REINDEER (292.6 m, $BHT_n = -1.28$ °C)	-1.1 ± 0.1[a]	-1.4 ± 0.1[a]	-1.456 ± 0.001
REINDEER (414.5 m, $BHT_n = 1.25$ °C)	1.19 ± 0.12[a]	1.12 ± 0.01[d]	1.215 ± 0.001
REINDEER (506 m, $BHT_n = 3.49$ °C)	3.4 ± 0.1[a]	3.38 ± 0.01[d]	3.472 ± 0.003
REINDEER (597.4 m, $BHT_n = 5.97$ °C)	5.85 ± 0.20	5.9 ± 0.1[a]	5.945 ± 0.01
MOKKA (18.3 m, $BHT_n = -15.371$ °C)	-15.3 ± 0.3	-15.7 ± 0.3[a]	-15.50 ± 0.01
MOKKA (30.5 m, $BHT_n = -15.016$ °C)	-14.6 ± 0.3	-15.0 ± 0.3	-15.117 ± 0.002
MOKKA (45.7 m, $BHT_n = -14.629$ °C)	-14.3 ± 0.3	-14.7 ± 0.3[a]	-14.717 ± 0.002
MOKKA (61 m, $BHT_n = -14.304$ °C)	-14.1 ± 0.3	-14.6 ± 0.3[a]	-14.387 ± 0.001
MOKKA (76.2 m, $BHT_n = -14.083$ °C)	-13.9 ± 0.3	-14.3 ± 0.3[a]	-14.126 ± 0.001
MOKKA (91.4 m, $BHT_n = -13.808$ °C)	-13.68 ± 0.24	-14.03 ± 0.25[a]	-13.970 ± 0.001
MOKKA (106.7 m, $BHT_n = -13.265$ °C)	-13.1 ± 0.3	-13.5 ± 0.3[a]	-13.2982 ± 0.0001
MOKKA (152.4 m, $BHT_n = -11.277$ °C)	-11.0 ± 0.2	-11.31 ± 0.22[a]	-11.36 ± 0.01
MOKKA (198.1 m, $BHT_n = -7.895$ °C)	-9.25 ± 0.14	-9.4 ± 0.3[d]	-9.85 ± 0.01
MOKKA (320 m, $BHT_n = -6.906$ °C)	-6.1 ± 0.3[b]	-7.22 ± 0.42[a]	-7.50 ± 0.01
MOKKA (441.9 m, $BHT_n = -2.361$ °C)	-1.83 ± 0.17[b]	-2.5 ± 0.2	-2.404 ± 0.001
P-RIVER (15.24 m, $BHT_n = -9.369$ °C)	-9.3 ± 1.1	-10 ± 1[a]	-9.58 ± 0.01
P-RIVER (30.48 m, $BHT_n = -9.167$ °C)	-9 ± 1	-10 ± 1	-9.2575 ± 0.0001
P-RIVER (45.72 m, $BHT_n = -9.052$ °C)	-9 ± 1	-10 ± 1	-9.43 ± 0.01
P-RIVER (60.96 m, $BHT_n = -8.957$ °C)	-9 ± 1	-10 ± 1	-9.2349 ± 0.0001
P-RIVER (91.44 m, $BHT_n = -8.771$ °C)	-8.5 ± 1.1	-10 ± 1	-9.51 ± 0.01
P-RIVER (152.4 m, $BHT_n = -8.124$ °C)	-7 ± 1	-8.8 ± 1.1	-8.7031 ± 0.0001
P-RIVER (304.81 m, $BHT_n = -5.462$ °C)	-4 ± 1	-5 ± 1	-8.5378 ± 0.0001
P-RIVER (335.28 m, $BHT_n = -4.935$ °C)	-3 ± 1	-5 ± 1	-7.6325 ± 0.0001
P-RIVER (396.24 m, $BHT_n = -4.039$ °C)	-3 ± 1	-4 ± 1	-4.241 ± 0.004
P-RIVER (579.12 m, $BHT_n = -0.778$ °C)	-1.0 ± 0.3	-0.58 ± 0.21[b]	-1.436 ± 0.001
P-RIVER (609.6 m, $BHT_n = -0.195$ °C)	0.03 ± 0.39	-0.57 ± 0.35	-1.797 ± 0.002
P − RIVER (640.08 m, $BHT_n = 0.761$ °C)	1 ± 1	1 ± 1	0.520 ± 0.001
P-RIVER (670.56 m, $BHT_n = 1.664$ °C)	2 ± 1	1.6 ± 0.3	$-0.018\,68 \pm 0.000\,02$
P-RIVER (701.04 m, $BHT_n = 2.885$ °C)	3 ± 1	2.7 ± 0.4	2.8578 ± 0.0003

[a] SFT (SRM) outlier.
[b] SFT (MM) outli er.
[c] SFT (LMM, MM and SRM) outlier.
[d] SFT (MM and SRM) outlier.

for SHBE (figure 15(B)). Finally, the results of significance tests of the data sets CJON and SHBE applied to the SFT estimations and TFT (figures 15(D) and (E)) do not show significant differences with a 95% confidence analysis. These results are in total agreement with the results shown in figures 15(A)–(C).

4.7. Comparative analysis between the estimated SFTs

Tables 13 and 14 report the SFT estimated by the log-transformation (T*ln*) method for the geothermal data sets, including the determined ones by the application of eight analytical methods with OLS and QR regression models. These tables were created with the purpose of emphasizing that, systematically, the analytical methods have a tendency to underestimate the SFT mainly when the OLS model is used. With this purpose in mind, the value of BHT_n was used as reference data to determine which analytical method and regression model underestimate the SFT. Theoretically, it is expected that for each BHT, the estimated SFT would not be less than the BHT_n data. This condition is clearly surpassed by the new method T*ln*, which seems to correct the obtained underestimations by some analytical methods commonly employed in geothermal, petroleum and permafrost applications. In fact, from the 314 geothermal SFT estimations (analytical methods) reported in tables 13 and 14, it was found that at least 76 estimations underestimate the SFT (25%).

In the case of the analyzed petroleum boreholes (table 15), it was found that from the 120 SFT estimations obtained by classical analytical methods, 34 estimations, 28%, clearly underestimate the SFT.

Finally, the estimated SFTs for the permafrost cases are reported in tables 16–18. In this application three exploration permafrost borehole (REINDEER, MOKKA, and P-RIVER) data sets were used, to which applying the HKM analytical method was not possible due to the own restrictions of the method and specifically, when the recovery time was longer ($\Delta t > 100$ h). Therefore, in these examples 470 SFT estimations were obtained by the analytical methods using OLS and QR models. In this kind of application, theoretically it is expected that the calculated SFT will be 'lower' than BHT_n, in relation to an analysis of the shown results (tables 16–18). It was found that approximately 43% of the estimations did not 'obey' this assumption. Systematically, the OLS model did not achieve such condition, and in some cases neither did the QR model.

Unfortunately, the observations mentioned earlier have not been validated due to the limited availability of information from the analyzed boreholes, and fundamentally, due to the fact that the accuracy and precision of the field measured data are unknown unlike those of the TFT synthetic data sets. These observations are based on the experience of working on this problem and international literature that fits in with the supposition (e.g. Dowdle and Cobb 1975, Deming 1989, Andaverde *et al* 2005). In the case of geothermal or petroleum boreholes that have presented problems of lost circulation during their drilling, it would be expected that the estimated SFT would not be less than the BHT_n at the particular depth where the data set is logged.

After completing the first comparative analysis between the calculated SFT by means of eight analytical methods and that corresponding to the new method T*ln* (tables 13–18), we proceeded to calculate the mean SFT from the analytical methods through the free software DODESYS (Verma *et al* 2008). Next, 'outlier' data using univariate data tests (Verma 2005) were identified and rejected statistically under the supposition that the SFT estimations calculated by the analytical methods obeyed a normal distribution. In tables 19–21 the numerical results for the average SFT are summarized, calculated through the analytical methods and the new method using the geothermal, petroleum and permafrost borehole data sets. In these tables, the acronyms OLS and QR were used to indicate the average SFT calculated by the analytical methods using the OLS and QR algorithms, respectively. The data marked with the superscript (a)–(d) indicate the 'outlier' data for the estimated SFT by the methods SRM and HKM and the groups of methods LMM–MM–SRM and MM–SRM, respectively. From this information we can infer that the SRM prediction provides, almost systematically, 'outlier' data values in the SFT estimations. In the geothermal applications (table 19), nine SFT estimations (22%) are underestimated according to the BHT_n data reference; from the petroleum cases five average SFTs (31%) are noted as underestimated; and finally, for the permafrost analysis, twenty-two average SFTs (44%) can be taken as underestimated in comparison to the data reference BHT_n.

Table 22. Obtained results from the *F*-test and Student's *t*-test between the comparison of the SFT calculated by the new method (T*ln*) and the average SFT from the analytical methods, using geothermal borehole data, and the synthetic data CJON, SHBE and CLAH.

	Methods	
Data sets	T*ln*-OLS	T*ln*-QR
Geothermal boreholes:		
CH-A$_4$	**H$_1$**	H$_0$
CH-A$_9$	**H$_1$**	**H$_1$**
CH-A$_{11}$	**H$_1$**	**H$_1$**
MXCO$_1$	H$_0$	H$_0$
MXCO$_2$	H$_0$	H$_0$
ITAL	H$_0$	H$_0$
PHIL	H$_0$	H$_0$
JAPN	H$_0$	H$_0$
CB-1 (994 m)	**H$_1$**	H$_0$
CB-1 (1494 m)	H$_0$	H$_0$
CB-1 (1987 m)	H$_0$	H$_0$
CB-1 (2583 m)	H$_0$	**H$_1$**
R #9-1	H$_0$	H$_0$
SGIL	H$_0$	H$_0$
ROUX	H$_0$	H$_0$
KELLEY	H$_0$	H$_0$
GT-2 (1595 m)	H$_0$	H$_0$
Synthetic data:		
CJON	H$_0$	H$_0$
SHBE	H$_0$	H$_0$
CLAH	H$_0$	H$_0$

Table 23. Obtained results from the *F*-test and Student's *t*-test between the comparison of the SFT calculated by the new method (T*ln*) and the average SFT from the analytical methods, using petroleum borehole data sets.

	Methods	
Data sets	T*ln*-OLS	T*ln*-QR
USAM	**H$_1$**	**H$_1$**
COST (1420 m)	H$_0$	**H$_1$**
COST (3710 m)	H$_0$	**H$_1$**
COST (4475 m)	H$_0$	**H$_1$**
MALOOB—456	**H$_1$**	**H$_1$**
MALOOB—309D	**H$_1$**	**H$_1$**
Franciacorta (3328 m)	**H$_1$**	**H$_1$**
BECU	H$_0$	H$_0$

Finally, to determine if significant differences exist between the average SFT from the analytical methods and the SFT calculated by the new method, *F*- and Student's *t*-tests were applied. The obtained results from this analysis are reported in tables 22–24, where T*ln*–OLS and T*ln*–QR indicate the statistical comparison between the SFT estimated by the new method and the average SFT from the analytical methods. H_0 and H_1 indicate in which cases significant differences between the SFTs exist or not. In table 22, it can be observed that from the 40 SFT estimations associated with geothermal boreholes,

Table 24. Obtained results from the *F*-test and Student's *t*-test between the comparison of the SFT calculated by the new method (T*ln*) and the average SFT from the analytical methods, using BHT and shut-in time logged in the permafrost boreholes REINDEER, MOKKA and P-RIVER.

	Methods	
Data sets	T*ln*-OLS	T*ln*-QR
REINDEER (18.3 m)	**H_1**	**H_1**
REINDEER (48.8 m)	H_0	**H_1**
REINDEER (79.2 m)	H_0	H_0
REINDEER (140.2 m)	**H_1**	**H_1**
REINDEER (201.2 m)	H_0	**H_1**
REINDEER (292.6 m)	**H_1**	H_0
REINDEER (414.5 m)	H_0	**H_1**
REINDEER (506 m)	H_0	**H_1**
REINDEER (597.4 m)	H_0	H_0
MOKKA (18.3 m)	H_0	H_0
MOKKA (30.5 m)	**H_1**	H_0
MOKKA (45.7 m)	**H_1**	H_0
MOKKA (61 m)	H_0	H_0
MOKKA (76.2 m)	H_0	H_0
MOKKA (91.4 m)	**H_1**	H_0
MOKKA (106.7 m)	H_0	H_0
MOKKA (152.4 m)	**H_1**	H_0
MOKKA (198.1 m)	**H_1**	**H_1**
MOKKA (320 m)	**H_1**	H_0
MOKKA (441.9 m)	**H_1**	H_0
P-RIVER (15.24 m)	H_0	H_0
P-RIVER (30.48 m)	H_0	H_0
P-RIVER (45.72 m)	H_0	H_0
P-RIVER (60.96 m)	H_0	H_0
P-RIVER (91.44 m)	H_0	H_0
P-RIVER (152.4 m)	H_0	H_0
P-RIVER (304.81 m)	**H_1**	**H_1**
P-RIVER (335.28 m)	**H_1**	**H_1**
P-RIVER (396.24 m)	**H_1**	H_0
P-RIVER (579.12 m)	**H_1**	**H_1**
P-RIVER (609.6 m)	**H_1**	**H_1**
P-RIVER (640.08 m)	H_0	H_0
P-RIVER (670.56 m)	**H_1**	**H_1**
P-RIVER (701.04 m)	H_0	H_0

seven significant differences were obtained (≈18%). From the petroleum application (table 23), the comparative analysis showed 69% with significant differences. Finally, in the case of the permafrost boreholes, 41% of the statistical comparisons showed significant differences (table 24).

From the global comparison analysis for all the temperature data sets, we can conclude that 35% from the 904 SFT estimations (tables 13–18) and 36% from 124 of the average SFTs (tables 19–21) were underestimated, and finally, the significant differences between the average SFT by the analytical methods and the SFT calculated by the T*ln* method are represented by 37% which represents 46 of the 124 estimations.

5. Conclusions

A new practical method based on logarithmic transformation regressions was successfully developed for the determination of the SFTs of geothermal, petroleum and permafrost boreholes. The new method involved the application of multiple linear and polynomial (from quadratic to eight-order) regression models to BHT and log-transformation (T*ln*) shut-in times. The best regression model was used for reproducing the asymptotic thermal recovery process of the boreholes with accuracy, and later used for the reliable determination of the SFT.

A geochemometric evaluation methodology was applied for demonstrating the efficiency and prediction capability of the new log-transformation method. Four statistical parameters (R^2, RSSn, Ext-Abs and %Dev) were successfully applied for the evaluation of the linear and non-linear regression models.

It was found that the temperature measurements and the shut-in times corrected by the log-transformation (T*ln*) were mostly better reproduced through non-linear regression models (e.g. Q(T*ln*1), Q(T*ln*2), Q(T*ln*3),…, EI(T*ln*1), EI(T*ln*2), EI(T*ln*3)). Nevertheless, in some particular cases where the thermal recovery shows quasi-linear tendencies, the linear regression models with T*ln* appeared as the best fitting tool.

All these assertions were supported based on the results of the 'best' coefficients to determine the regression models (R^2), lower residuals (RSSn), numerical extrapolation (Ext-Abs) and more accurate simulations given by the evaluation parameter %Dev.

It is important to emphasize that in the geothermal or petroleum borehole analysis, the definition criterion of the convergence parameter for the new method was %Dev $\leqslant$ 0.01 for temperature data sets above 100 °C, whereas for temperatures in the interval 10 $\leqslant$ BHT (°C) $\leqslant$ 100, a value of %Dev $\leqslant$ 0.001 was adopted. In the case of permafrost systems, the parameter %Dev $\leqslant$ 0.001.

As part of the new numerical methodology developed, it was also found that the availability of data sets with a high number of measurements ($n > 10$) provides the possibility to obtain a major number of regression models (GRM (T*ln*)) for a much better analysis, which will provide the most reliable SFT estimations. It is important to note that the number and the quality of the measured data also play an important role for a more efficient application of the new method.

According to the accuracy analysis, it was demonstrated that the SFT predictions from the new developed method present average deviations less than 3%.

The difficulties that prevent an integral evaluation and a better selection of analytical and empirical methods are basically due to the following factors: (i) the limited number of BHT measurements gathered in the different applications (in order to be highly desirable there must be at least 30 measurements, a situation that can be viably reached with current measuring technology, such as optical or digital fiber); (ii) the limited number of synthetic data sets of different temperature ranges, whether high, medium or low, and knowledge of their TFT for a more accurate analysis; and (iii) reassessment of some of the physical—conceptual—and mathematical models of simplified analytical methods due to the presence of complex heat transfer phenomena that form part of these thermal disturbance processes.

Inside this context of difficulties and limitations, the T*ln* method offers several technical and practical advantages over the existing analytical methods, among which the following stand out: (i) knowledge of circulation time is not required, as it is a physical parameter that is very hard to determine with high precision and accuracy under field conditions; (ii) neither are the thermophysical and transport property data from the formation, cementation, mud and drilling tubing required; and (iii) the input data on the BHT and thermal recovery time (shut-in time) measurements are also required.

Finally, we can also conclude that the newly developed empirical method (T*ln*) for SFT calculation in geo-systems achieves the expected theoretical conditions and results, and that it makes for a practical, useful and effective tool to use in these kinds of tasks. Also it can have additional applications in the development and calibration of numerical simulators to reproduce the thermal histories of boreholes and/or the surrounding formations.

Acknowledgments

The first author wants to thank CONACyT (México) for the PhD, postdoctoral and the Chair-Program scholarships. The authors want to give special thanks to Dr S P Verma, for all the intellectual contributions and technical suggestions, which greatly helped them to improve this work. The authors are also grateful to the anonymous reviewers for their helpful and constructive comments on an earlier version of the paper. Finally, the second author also acknowledges the CONACyT fellowship program and the CIICAp-UAEM Institution for supporting his sabbatical year.

References

Albright J N 1975 *Temperature Measurements in the Precambrian Section of Geothermal Test Hole* vol 2 (Los Alamos, NM: Los Alamos Scientific Laboratory of the University of California) pp 1–11

Andaverde J, Verma S P and Santoyo E 2005 Uncertainty estimates of static formation temperatures in boreholes and evaluation of regression models *Geophys. J. Int.* **160** 1112–22

Aragon A, Garcia A, Baca A and Gonzalez E 1999 Comparison of measured and simulated pressure and temperature profiles in geothermal wells *Geofis. Int.* **38** 35–42

Ascencio F, Garcia A, Rivera J and Arellano V 1994 Estimation of undisturbed formation temperatures under spherical-radial heat flow conditions *Geothermics* **23** 317–26

Ascencio F, Samaniego F and Rivera J 2006 Application of a spherical-radial heat transfer model to calculate geothermal gradients from measurements in deep boreholes *Geothermics* **35** 70–8

Baskerville G L 1972 Use of logarithmic regression in the estimation of plant biomass *Can. J. Forest Res.* **2** 49–53

Barelli A, Carsana C G, Lombardi C and Maran L 1994 Prediction of geothermal well pressure and temperature profiles *Geothermics* **23** 339–53

Barelli A and Palama A 1981 A new method for evaluating formation equilibrium temperature in holes during drilling *Geothermics* **10** 95–105

Bassam A, Santoyo E, Andaverde J, Hernández J A and Espinoza-Ojeda O M 2010 Estimation of static formation temperatures in geothermal wells by using an artificial neural network approach *Comput. Geosci.* **36** 1191–9

Beardsmore G R and Cull J P 2001 *Crustal Heat Flow* (Harlow: Cambridge University Press) p 324

Beirute R M 1991 A circulating and shut-in well-temperature-profile simulator *J. Pet. Technol.* **43** 1140–6

Bevington P R and Robinson D 2003 *Data Reduction and Error Analysis for the Physical Sciences* 3rd edn (New York: McGraw Hill) p 320

Bodri L and Cermak V 2007 *Borehole Climatology: a New Method on How to Reconstruct Climate* 1st edn (Oxford: Elsevier) p 335

Brennand A W 1984 A new method for the analysis of static formation temperature tests *Proc. of the 6th New Zealand Geothermal Workshop (New Zealand)* pp 45–47

Cao S, Lerche I and Hermanrud C 1988a Formation temperature estimation by inversion of borehole measurements *Geophysics* **53** 979–88

Cao S, Hermanrud C and Lerche I 1988b Estimation of formation temperature from bottom-hole temperature measurements: COST #1 well, Norton Sound, Alaska *Geophysics* **53** 1619–21

Cao S and Lerche I 1990 Formation pressure estimation *J. Pet. Sci. Eng.* **4** 223–33

Cooper L R and Jones C 1959 The determination of virgin strata temperatures from observations in deep survey boreholes *Geophys. J. R. Astron. Soc.* **2** 116–31

Crosby G W 1977 Prediction of final temperature *Proc. of the 3rd Workshop on Geothermal Reservoir Engineering (Stanford University, Stanford, CA)* pp 89–95

Clow G and Lachenbruch A 1998 Borehole locations and permafrost depths, Alaska, USA International Permafrost Association, Data and Information Working Group, comp. Circumpolar Active-Layer Permafrost System (CAPS) version 1.0 (CD-ROM available from National Snow and Ice Data Center nsidc@kryos.colorado.edu) (Boulder: NSIDC, University of Colorado at Boulder)

Davis M G, Chapman D S and Harris R N 2011 Geothermal record of climate change *Encyclopedia of Solid Earth Geophysics* ed H K Gupta (Berln: Springer) pp 415–20

Da-Xin L 1986 Non-linear fitting method of finding equilibrium temperature from BHT data *Geothermics* **15** 657–64

Deming D 1989 Application of bottom-hole temperature corrections in geothermal studies *Geothermics* **18** 775–86

Dowdle W L and Cobb W M 1975 Static formation temperature from well logs—an empirical method *J. Pet. Tech.* **27** 1326–30

Drury M J 1984 On a possible source of error in extracting equilibrium formation temperatures from borehole BHT data *Geothermics* **13** 175–80

Eppelbaum L V and Kutasov I M 2011 Determination of the formation temperature from shut-in logs: estimation of the radius of thermal influence *J. Appl. Geophys.* **73** 278–82

Espinosa-Paredes G and Garcia-Gutierrez A 2003 Estimation of static formation temperatures in geothermal wells *Energy Convers. Manage.* **44** 1343–55

Espinosa-Paredes G, Morales-Díaz A, Olea-González U and Ambriz-Garcia J J 2009 Application of a proportional-integral control for the estimation of static formation temperatures in oil wells *Mar. Pet. Geol.* **26** 259–68

Espinoza-Ojeda O M 2011 Evaluación de modelos matemáticos y de transferencia de calor en el desarrollo de un nuevo método analítico para la determinación de temperaturas estabilizadas en sistemas geoenergéticos (pozos geotérmicos, petroleros y permafrost) *PhD Thesis* Centro de Investigación en Energía (Sistemas Energéticos—Geoenergía), Universidad Nacional Autónoma de México, Temixco, Morelos, 258pp

Espinoza-Ojeda O M, Santoyo E and Andaverde J 2011 A new look at the statistical assessment of approximate and rigorous methods for the estimation of stabilized formation temperatures in geothermal and petroleum wells *J. Geophys. Eng.* **8** 233–58

Fertl W H and Timko D J 1972 How downhole temperatures, pressures affect drilling, part 2: detecting and evaluating formation pressures *World Oil* pp 45–50
Garcia A, Santoyo E, Espinosa G, Hernandez I and Gutierrez H 1998 Estimation of temperatures in geothermal wells during circulation and shut-in in the presence of lost circulation *Transp. Porous Media* **33** 103–27
Gonzalez Partida E, Garcia Gutierrez A and Torres Rodriguez V 1997 Thermal and petrologic study of the CH-A well from the Chipilapa-Ahuachapan geothermal area, El salvador *Geothermics* **26** 701–13
Goutorbe B, Lucazeau F and Bonneville A 2007 Comparison of several BHT correction methods: a case study on an Australian data set *Geophys. J. Int.* **170** 913–22
Grant M A, Bixley P F and Donaldson I G 1983 Internal flows in geothermal wells: their identification and effect on the wellbore temperature and pressure profiles *Soc. Pet. Eng. J.* **23** 168–76
Harris R N and Chapman D S 1997 Borehole temperature and a baseline for 20th-century global warming estimates *Science* **275** 1618–21
Hasan A R and Kabir C S 1994 Determination of static reservoir temperature from transient data following mud circulation *SPE Drill. Completion* **9** 17–24
Horner D R 1951 Pressure build-up in wells *Proc. of the 3rd World Petroleum Congress (The Hague, The Netherlands)* pp 503–21
Howarth R J and Earle S A M 1979 Application of a generalized power transformation to geochemical data *J. Int. Assoc. Math. Geol.* **11** 45–62
Huang S, Pollack H N and Shen P Y 2000 Temperature trends over the past five centuries reconstructed from borehole temperatures *Nature* **403** 756–8
Hyodo M and Takasugi S 1995 Evaluation of the curve-fitting method and the Horner-plot method for estimation of the true formation temperature using temperature recovery logging data *Proc. of the 20th Workshop on Geothermal Reservoir Engineering (Stanford University, Stanford, CA, 24–26 January)* pp 23–9
Jones F W, Rahman M and Leblanc Y 1984 A 3D numerical bottom-hole temperature stabilization model *Geophys. Prospect.* **32** 18–36
Keller H H, Couch E J and Berry P M 1973 Temperature distribution in circulating mud columns *Soc. Pet. Eng. J.* **13** 23–30
Kutasov I M 1999 *Applied Geothermics for Petroleum Engineers* 1st edn (Amsterdam: Elsevier) p 347
Kutasov I M and Eppelbaum L V 2005 Determination of formation temperature from bottom-hole temperature logs-a generalized Horner method *J. Geophys. Eng.* **2** 90–6
Kutasov I M and Eppelbaum L V 2010 A new method for determining the formation temperature from bottom-hole temperature logs *J. Pet. Gas Eng.* **1** 1–8
Kutasov I M and Eppelbaum L V 2011 Recovery of the thermal equilibrium in deep and super deep wells: utilization of measurements while drilling data *Proc. of the 36th Workshop on Geothermal Reservoir Engineering (Stanford University, Stanford, CA, 31 January–2 February)* p 7
Lachenbruch A H and Marshall B V 1986 Changing climate: geothermal evidence from permafrost in the Alaskan Arctic *Science* **234** 689–96
Leblanc Y, Lam H-L, Pascoe L J and Jones F W 1982 A comparison of two methods of estimating static formation temperature from well logs *Geophys. Prospect.* **30** 348–57
Leblanc Y, Pascoe L J and Jones F W 1981 The temperature stabilization of a borehole *Geophysics* **46** 1301–3
Lee T 1982 Estimation of formation temperature and thermal property from dissipation of heat generated by drilling *Geophysics* **47** 1577–84
Luheshi M N 1983 Estimation of formation temperature from borehole measurements *Geophys. J. R. Astron. Soc.* **74** 747–76
Manetti G 1973 Attainment of temperature equilibrium in holes during drilling *Geothermics* **2** 94–100
Middleton M F 1979 A model for bottom-hole temperature stabilization *Geophysics* **44** 1458–62
Middleton M F 1982 Bottom-hole temperature stabilization with continued circulation of drilling mud *Geophysics* **47** 1716–23
Olea-González U, Bautista-Pastrana D and Espinosa-Paredes G 2008 Transporte de calor con pérdida de circulación en un pozo-formación de la zona marina, al aplicar un método inverso *Proc. of the Congreso Mexicano Del Petróleo* pp 1–10
Olea-González U and García-Gutiérrez A 2008 Estimation of static formation temperatures in geothermal and oil well by inversion of logged temperatures *Geotherm. Resour. Counc. Trans.* **32** 53–6
Olea-González U, Vázquez-Rodríguez A, García-Gutiérrez A and Anguiano-Rojas P 2007 Estimación de temperaturas de formación en yacimientos: Método inverso *Rev. Mex. Ing. Quím.* **6** 65–74
Pasquale V, Chiozzi P, Gola G and Verdoya M 2008 Depth-time correction of petroleum bottom-hole temperatures in the Po Plain, Italy *Geophysics* **73** E187–96
Porkhial S, Salehpour M, Ashraf H and Jamali A 2015 Modeling and prediction of geotherma lreservoir temperature behavior using evolutionary design of neural networks *Geothermics* **53** 320–27
Raymond L R 1969 Temperature distribution in a circulating drilling fluid *J. Pet. Technol.* **21** 333–41
Ribeiro F B and Hamza V M 1986 Stabilization of bottom-hole temperature in the presence of formation fluid flows *Geophysics* **51** 410–13
Roux B, Sanyal S K and Brown S 1980 An improved approach to estimating true reservoir temperature from transient temperature data *Proc. of the SPE California Regional Meeting (Los Angeles, CA, 9–11 April)* pp 1–8
Santoyo E, Garcia A, Espinosa G, Hernandez I and Santoyo S 2000 STATIC_TEMP: a useful computer code for calculating static formation temperatures in geothermal wells *Comput. Geosci.* **26** 201–17
Schoeppel R J and Gilarranz S 1966 Use of well log temperatures to evaluate regional geothermal gradients *J. Pet. Technol.* **18** 667–73
Shen P Y and Beck A E 1986 Stabilization of bottom hole temperature with finite circulation time and fluid flow *Geophys. J. R. Astron. Soc.* **86** 63–90
StatSoft Inc. 2003 *STATISTICA (Data Analysis Software System)* Ver 6 www.statsoft.com
Stevens L 2000 Pressure, temperature and flow logging in geothermal wells *Proc. of the World Geothermal Congress (Kyushu-Tohoku, Japan, 28 May–10 June)* pp 2435–7
Sulastri M and Andriany S S 2015 Wells declivity temperature geothermal field Bora-Sigi, Central Sulawesi, Indonesia *Engineering Geology for Society and Territory* vol 1 (Berlin: Springer) pp 373–8
Taylor A E, Burgess M M, Judge A S and Allen V S 1982 Canadian geothermal data collection—Northern Wells 1981 *Earth Physics Branch, Energy, Mines and Resources, Canada* (*Geothermal Series* vol 13) p 153
Timko D J and Fertl W H 1972 How downhole temperatures, pressures affect drilling. Part VII: the shale resistivity ratio—a valuable tool for making economic drilling decisions *World Oil* pp 59–63
Vaz de Medeiros Rangel M G 2014 Temperature model and tracer test analysis for the Ribeira Grande geothermal system, São Miguel Island, Azores *UNU-GTP Geothermal Training Programme (United Nations University, Iceland)* vol 29 pp 615–42 (reports 2014)
Verma S P 2009 Evaluation of polynomial regression models for the Student *t* and Fisher *F* critical values, the best interpolation equations from double and triple natural logarithm

transformation of degrees of freedom up to 1000, and their applications to quality control in science and engineering *Rev. Mex. Cienc. Geol.* **26** 79–92

Verma S P 2015 Monte Carlo comparison of conventional ternary diagrams with new log-ratio bivariate diagrams and an example of tectonic discrimination *Geochem. J.* **49** 393–412

Verma S P and Agrawal S 2011 New tectonic discrimination diagrams for basic and ultrabasic volcanic rocks through log-transformed ratios of high field strength elements and implications for petrogenetic processes *Rev. Mex. Cienc. Geol.* **28** 24–44

Verma S P, Andaverde J and Santoyo E 2005 Error propagation in estimates of static formation temperature in boreholes *Proc. of the Heat Transfer in Components and Systems for Sustainable Energy Technologies (Grenoble, France, 5–7 April)* pp 1–8

Verma S P, Andaverde J and Santoyo E 2006a Application of the error propagation theory in estimates of static formation temperatures in geothermal and petroleum boreholes *Energy Convers. Manage.* **47** 3659–71

Verma S P and Quiroz-Ruiz A 2008 Critical values for 33 discordancy test variants for outliers in normal samples of very large sizes from 1000–30 000 and evaluation of different regression models for the interpolation and extrapolation of critical values *Rev. Mex. Cienc. Geol.* **25** 369–81

Verma S P, Quiroz-Ruiz A and Díaz-González L 2008 Critical values for 33 discordancy test variants for outliers in normal samples up to sizes 1000, and applications in quality control in Earth sciences *Rev. Mex. Cienc. Geol.* **25** 82–96

Waples D W and Ramly M 1995 A simple statistical method for correcting and standardizing heat flows and subsurface temperatures derived from log and test data *Bull. Geol. Soc. Malays. Spec. Publ.* **37** 253–67

Waples D W and Ramly M 2001 A statistical method for correcting log-derived temperatures *Pet. Geosci.* **7** 231–40

Waples D W, Pacheco J and Vera A 2004a A method for correcting log-derived temperatures in deep wells, calibrated in the Gulf of Mexico *Pet. Geosci.* **10** 239–45

Waples D W and Pederson M R 2004 Evaluation of Horner plot-corrected log-derived temperatures in the Danish Graben, North Sea *Nat. Resour. Res.* **13** 223–7

Waples D W, Pederson M R and Kuijpers P 2004b Correction of single log-derived temperatures in the Danish Central Graben, North Sea *Nat. Resour. Res.* **13** 229–39

Wong-Loya J A, Andaverde J and Santoyo E 2012 A new practical method for the determination of static formation temperatures in geothermal and petroleum wells using a numerical method based on rational polynomial functions *J. Geophys. Eng.* **9** 711–28

Wong-Loya J A, Andaverde J A and del Rio J A 2015 Improved method for estimating static formation temperatures in geothermal and petroleum wells *Geothermics* **57** 73–83

Yang M, Li X, Deng J, Meng Y and Li G 2015 Prediction of wellbore and formation temperatures during circulation and shut-in stages under kick conditions *Energy* **91** 1018–29